



Seasonal variation and short-term variability during SSWs of the gravity wave momentum flux

Masterarbeit
angefertigt am Institut für Physik der
Mathematisch-Naturwissenschaftlichen Fakultät der
Universität Rostock
und am Leibniz-Institut für Atmosphärenphysik in
Kühlungsborn

von Helen Schneider, geb. am 22. September 1989 in Rostock

1. Prüfer: Prof. Jorge Chau, Universität Rostock
2. Prüfer: Dr. Gunter Stober, Universität Rostock

Rostock, den 26. August 2016

Abstract

Gravity waves play an important role in the dynamics of the mesosphere as they are, for example, responsible for the paradox of the extreme cold summer mesopause at polar latitudes. To investigate the influence of gravity waves on the background wind in the mesosphere on a short and long term variability, the gravity wave activity, gravity wave momentum flux and mean zonal wind is considered using meteor radar data at Andenes ($69^{\circ}N, 16^{\circ}E$) and Juliusruh ($54^{\circ}N, 13^{\circ}E$). The gravity wave activity is determined by the variance of the residual radial velocity and the gravity wave momentum flux is calculated by the method introduced by *Hocking* (2005).

The short term variability of the gravity wave activity and momentum flux is considered during sudden stratospheric warmings (SSWs). The results show, that the gravity wave activity is enhanced before the SSW onset and weakens during the SSW. The position of the polar vortex has a strong impact on the gravity wave activity as well. Furthermore the mesospheric gravity wave momentum flux changes during a SSW due to the SSW induced wind reversal in the stratosphere, which supports the theory of stratospheric gravity wave filtering. Moreover, interactions between mean zonal wind and momentum flux are verified.

The seasonal variation of the gravity wave activity and momentum flux is considered using the composite analysis. In general the gravity wave momentum flux is anti-correlated to the observed mean zonal wind. However, in years with major SSWs, i.e. the zonal wind reverses at 10hPa during the SSW, the gravity wave momentum flux shows deviations from the anti-correlation below 85 km which cannot only be explained by SSW effects. In all years a strong interaction between the gravity wave momentum flux and the mean zonal wind is apparent during the summer months at heights above 90 km.

Zusammenfassung

Schwerewellen spielen eine bedeutende Rolle in der Dynamik der Mesosphäre, da sie, zum Beispiel, für das Paradoxon der extrem kalten Sommermesopause in polaren Breiten verantwortlich sind. Um den Einfluss von Schwerewellen auf den Hintergrundwind in der Mesosphäre auf Kurz- und Langzeitvariabilität zu untersuchen, wird die Schwerewellenaktivität, der Schwerewellenimpulsfluss und der Zonalwind mit Hilfe von Meteor Radar Daten aus Andenes ($69^{\circ}N, 16^{\circ}O$) und Juliusruh ($54^{\circ}N, 13^{\circ}O$) betrachtet. Die Schwerewellenaktivität wird aus der Varianz der residualen radialen Geschwindigkeiten bestimmt und der Schwerewellenimpulsfluss mit der von *Hocking* (2005) vorgestellten Methode berechnet.

Die Kurzzeitvariabilität der Schwerewellenaktivität und des Schwerewellenimpulsflusses wird während sogenannten plötzlichen Stratosphären Erwärmungen (SSW) untersucht. Die Ergebnisse zeigen, dass die Schwerewellenaktivität vor dem Beginn der SSW erhöht ist und sich während der SSW abschwächt. Zusätzlich hat die Position des Polarwirbels einen starken Einfluss auf die Schwerewellenaktivität. Darüber hinaus ändert sich der Schwerewellenimpulsfluss während einer SSW, da durch die SSW eine Windumkehr in der Stratosphäre hervorgerufen wird. Dies unterstützt die Theorie, dass Schwerewellen durch den zonalen Grundstrom in der Stratosphäre gefiltert werden. Außerdem können auch Wechselwirkungen zwischen zonalem Grundstrom und Schwerewellenimpulsfluss in der Mesosphäre verifiziert werden.

Der mittlere Jahresgang der Schwerewellenaktivität und des Schwerewellenimpulsflusses wird mit Hilfe der Kompositeanalyse betrachtet. Im Allgemeinen ist der Schwerewellenimpulsfluss antikorreliert zum beobachteten zonalen Grundstrom. Dennoch zeigt der Schwerewellenimpulsfluss, in Jahren mit starken SSWs (Windumkehrin 10 hPa), Abweichungen von der Antikorrelation unterhalb von 85 km, was nicht nur durch Effekte der SSW erklärt werden kann. In allen Jahren tritt eine deutliche Wechselwirkung zwischen Schwerewellenimpulsfluss und zonalem Grundstrom während der Sommermonate oberhalb von 90 km auf.

Contents

1	Introduction	1
2	Theoretical background	5
2.1	Atmosphere	5
2.2	Gravity waves	7
2.3	Planetary waves	11
2.4	Atmospheric tides	15
2.5	Sudden stratospheric warming (SSW)	17
3	Instruments and data	20
3.1	Basic principles of the radar technology	20
3.2	The meteor radar	21
3.3	Determination of the neutral wind	23
3.4	Wind fitting	24
3.5	Calculation of the gravity wave momentum flux	26
3.6	Parameter variations	27
3.6.1	Number of meteors	27
3.6.2	Averaging windows and steps	28
3.6.3	Weighting of the calculated momentum flux	32
4	Measurements	33
4.1	Identification of a SSW	33
4.2	Gravity wave activity and momentum flux around SSWs	34
4.2.1	Gravity wave activity	34
4.2.2	Momentum flux	38
4.3	Annual variation	45
5	Discussion	49
5.1	Gravity wave activity and momentum flux around SSWs	49
5.1.1	Gravity wave activity during SSW periods	49
5.1.2	Gravity wave momentum flux during SSW periods	51
5.2	Annual variation of the gravity wave momentum flux	55

6	Conclusion	58
7	Appendix	63
8	Bibliography	71

1 Introduction

The earth is surrounded by a gas layer called atmosphere. Due to complex chemical and physical processes the composition of the atmosphere varies with height, latitude and longitude. The varying concentration of trace gases at specific heights in the atmosphere results in a varying absorption of solar radiation (e.g. *Forbes (1995)*). This leads to altering temperatures with height. Regarding to the altering vertical temperature gradient the atmosphere is composed of several layers. The troposphere (0-15 km) has a negative temperature gradient, the stratosphere (15-50 km) a positive temperature gradient, the mesosphere (50-85 km) has a negative temperature gradient again and the thermosphere (>85 km) a positive temperature gradient. The density of the atmosphere is described by the barometric formula (eq. 2.1) and decreases exponentially with increasing height. Hence the lowest layer, the troposphere, is the most dense. It contains nearly 80 percent of the atmosphere's mass (*McGraw (2009)*). Moreover the troposphere contains most of the water vapor of the atmosphere. The troposphere is also the layer where most weather phenomena take place. Only 60 km above, in the upper mesosphere, the density has decreased by approximately 4 orders of magnitude (~ 0.01 hPa at 75 km). The mesosphere is a dynamical active region in spite of the lower density. The variability of the mesosphere for example, is given by the occurrence of noctilucent clouds (NLC) or polar mesospheric summer echoes (PMSE) in the polar summer mesosphere. NLC and PMSE are attributed to the generation of ice particles (e.g. *Hervig et al. (2001)*, *Rapp and Lübken (2003)*). Although the mesosphere contains almost no water vapor, ice particles are still generated and NLC and PMSE can be observed. This is related to the low pressure at mesospheric heights and the low temperatures, which reach minimum values of the entire atmosphere in the polar summer mesosphere (*Lübken and von Zahn (1991)*). The contradiction of minimum temperatures in the summer mesosphere in spite of higher solar radiation in summer than in winter, can be explained by the residual circulation from summer pole to winter pole in upper mesospheric heights (>75 km) which is driven by gravity waves (e.g. *Holton and Alexander (2000)*).

Gravity, planetary and tidal waves are the most important atmospheric waves at mid- and polar latitudes. They can be identified by fluctuations in density, pres-

sure, temperature and wind. The different wave types distinguish in their restoring forces, generation mechanisms as well as temporal and spatial scales. Planetary- and tidal waves are of global extend whereas locally generated gravity waves are small scaled (*Placke (2014)*). Gravity waves are mainly generated in the troposphere e.g. due to orography, convection or geostrophic adjustments (*Fritts and Alexander (2003)*). After the generation, the waves propagate horizontally as well as vertically. Due to the exponentially decreasing density, the amplitudes of those waves grow exponentially with increasing altitudes. At a critical height, their amplitudes become too large and the waves become instable and they break (*Lindzen (1981)*). Furthermore gravity waves can be filtered by the zonal wind. If the horizontal phase velocity of a gravity wave equal the mean zonal wind velocity, the vertical wavelength becomes zero and the wave breaks (*Brasseur and S.Solomon (2005)*). As the waves break, their kinetic energy and momentum flux are released. This leads to a heating of the surrounding atmosphere and an acceleration or deceleration of the mean flow, due to the momentum flux induced wave drag (*Fritts and Alexander (2003)*).

Due to the transmission of energy and momentum flux while wave breaking, atmospheric waves provide an essential contribution to the coupling between the atmospheric layers. Since those coupling processes are quite complex, it is challenging to separate and analyse the different effects. The most impressive and prominent coupling processes induced by planetary waves is the sudden stratospheric warming (SSW). It is characterized by a sudden stratospheric warming and simultaneous mesospheric cooling. Additionally, the zonal wind weakens or even reverses in cases of a major SSW. A SSW was observed for the first time by *Scherhag (1952)*. According to *Matsuno (1971)*, the reason of a SSW is the interaction of planetary waves with the background wind. SSWs are a winter phenomenon, since planetary waves can vertically propagate into the middle atmosphere only when eastward zonal wind dominates (*Charney and Drazin (1961)*). Gravity waves on the one hand cause the mesospheric cooling (*Labitzke (1972)*) but are also influenced by the changed wind conditions in the stratosphere as they results in changed filter conditions.

There are many studies which approach the issue of gravity waves in relation to SSWs-induced changes in the mean zonal wind and moreover the position relative to the polar vortex. By Lidar measurements during the period from 1993-1996 *Whiteway et al.* (1997) observed that the gravity wave activity has its maximum at the edge of the polar vortex, its minimum inside of the polar vortex close to the core and intermediate outside the polar vortex. This is supported by satellite observations presented by *Wang and Alexander* (2009) as well as by ECMWF model analyses in *Yamashita et al.* (2010). Furthermore an enhanced gravity wave activity in the stratosphere (*Wang and Alexander* (2009)) and a suppressed gravity wave activity in the mesosphere (*Wang and Alexander* (2009) and *Hoffmann et al.* (2007)) during a SSW is observed. Only a few studies discuss the gravity wave momentum flux (e.g. *Andrioli et al.* (2013)) or the gravity wave momentum flux during SSWs (*de Wit et al.* (2014)). In general, the past studies paid more attention to the stratospheric dynamical processes during a SSW, which are understood quite well. Whereas the SSW response due to gravity waves in the mesosphere and lower thermosphere (MLT) have not yet been fully studied (e.g. *Hoffmann et al.* (2007), *de Wit et al.* (2014)).

Therefore the present thesis deals with the gravity wave activity as well as the mean zonal wind and the gravity wave momentum flux during SSWs in the mesosphere. In addition, the annual variation of mesospheric mean zonal wind and gravity wave momentum flux are analysed in composite studies. The mesospheric wind and gravity wave momentum flux were determined by data provided by the meteor radars in Andenes and Juliusruh.

In chapter 2 the theoretical background is introduced including fundamentals regarding to the atmosphere, atmospheric waves and the SSW. In chapter 3 the measuring instruments are introduced and the calculation of wind and momentum flux are described in more detail. Furthermore parameter variations are considered. Chapter 4 contains the results for the above described research focuses. For realisation five major warming events were considered separately as well as in a composite. Moreover composites of the annual variations of the mean zonal wind and gravity wave momentum flux are created including the years 2004-2014. Subsequently the results are discussed in chapter 5. The discussion includes the

influence to gravity wave activity by a SSW. Thereby the polar vortex position was also taken into account. Furthermore it is examined if the variation of the mesospheric momentum flux during SSW supports the theory of stratospheric wave filtering and if the variation of the mean zonal wind is influenced by the momentum flux due to the induced wave drag. In the end follows a comparison of the composite of mean zonal wind and momentum flux for years with and without a major warming. Finally the conclusion of the most important results are presented in chapter 6.

2 Theoretical background

2.1 Atmosphere

The atmosphere is the gas layer which surrounds the earth. It mainly consists of nitrogen (78,08%), oxygen (20,95%) and atmospheric tracegases as argon, water vapor, ozone and carbone dioxide. With its nonlinear processes and strong variabilities the atmosphere is a very complex system. The atmosphere in rest can be described by the barometric formula:

$$\frac{\partial p}{\partial z} = -\rho \cdot g \quad (2.1)$$

where p is pressure, z is height, ρ is density and g represents the earth acceleration. Replacing the density over the ideal gas law and solving the differential equation yields:

$$p = p(z_0) \cdot \exp\left(-\int_{z_0}^z \frac{Mg(z')}{RT(z')} dz'\right). \quad (2.2)$$

Since the atmosphere is approximatly well mixed up to 90 km height the molar mass M doesn't change with z . Assuming now an isotherm atmosphere the equation 2.2 simplifies to:

$$p(z) = p(z_0) \cdot \exp\left(-\frac{z - z_0}{H}\right) \quad (2.3)$$

With $H = \frac{k_B T}{mg}$ as scale height, where k_B is the Boltzmann constant, T the temperature and m the mass. So the pressure in the atmosphere decreases with a factor $1/e$ per scale height.

The atmosphere is subdivided in different layers based on the vertical temperature profile (see fig. 1). The troposphere reaches from zero to ten km in high latitudes or up to fifteen kilometres in the equatorial area and is characterized by a negative temperature gradient. In the troposphere most weather phenomena take place. The upper limit of the troposphere is called tropopause. Above the stratosphere it follows, ranging from 15 to 50 km. The stratosphere contains most of the ozone proportion in the atmosphere. This results in a warming in this area, and thus the temperature gradient is positive. Above the stratosphere the stratopause is

located, which is the limit between stratosphere and mesosphere. The Mesosphere extends approximately from 50 km to 95 km. In the mesosphere the density decreases and the absorbed solar radiation becomes insufficient to balance the cooling into space. Following, the temperature gradient becomes negative again. It follows the mesopause and from 100 km upward the thermosphere begins. Based on photolysis of molecular oxygen the temperature gradient is positive (*Placke (2014)*). As you can see in figure 1, the temperature profile for winter (blue) has lower values as for summer in the troposphere and stratosphere as it was expected. However, in the mesosphere the temperatures in summer (red) are around 40°C lower than in winter (*Lübken and von Zahn (1991)*). This circumstance seems paradoxical, since the highest solar radiation rates occur during summer. It can be explained by the gravity wave-driven residual circulation from summer to winter pole, which is characteristic for the MLT-region (mesosphere-lower thermosphere) (*Holton and Alexander (2000)*). The MLT-region begins at around 60 km and reaches up to 110 km. Especially waves are responsible for dynamic processes in the MLT-region. Waves are marked for example in fluctuations of wind, density or temperature. The most important wave types are gravity waves, planetary waves and tides. Those wave types are described in detail below. Gravity waves are small scaled and their restoring force is the gravity (*Fritts and Alexander (2003)*). The latter two wave types are large scaled. The Coriolis force acts as restoring force for planetary waves. Tides include solar tides, excited by differential solar heating and lunar tides, which are caused gravitationally (*Forbes (1995)*). All wave types have in common that they just exist in stable stratified layers.

In figure 2 the atmospheric zonal wind profile is shown. In summer the prevailing winds are negative (westward, easterly) and in winter positive (eastward, westerly) up to the upper mesosphere. That annual wind variation determines the vertical propagation of the atmospheric waves, due to filtering conditions. So there are season depending variations of the waves, which affect among other things the MLT dynamics. Those are described in more detail below.

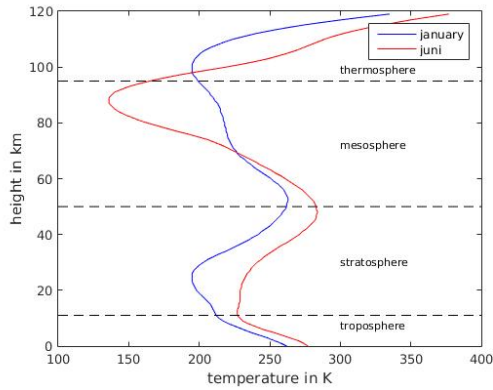


Figure 1: typical vertical temperature profile for winter (blue) and summer (red) (MISIS reference atmosphere)

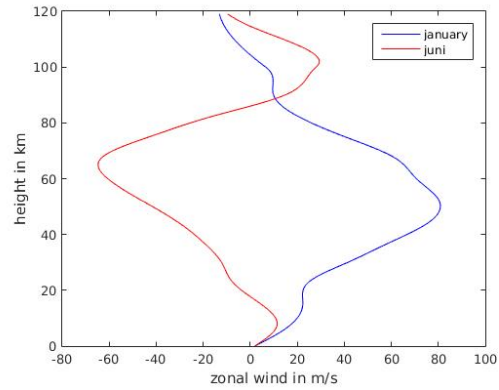


Figure 2: typical vertical zonal mean wind profile for winter (blue) and summer (red) (hwm07 reference atmosphere)

2.2 Gravity waves

A gravity wave can be imagined as an air parcel which is deflected from its rest position by e.g. an overflow of a mountain. In a stable stratified atmosphere the air parcel oscillates adiabatically. The atmosphere is stable stratified when the dry adiabatic temperature gradient, Γ , is larger than the vertical temperature gradient.

$$\Gamma > \frac{dT}{dz} \quad \hat{=} \quad \text{stable} \quad (2.4)$$

$$\text{with } \Gamma = -\frac{g}{c_p} = 9.8 \frac{K}{km}$$

Where c_p is the specific heat at constant pressure.

The frequency of the air parcel oscillation is described by the buoyancy frequency N (e.g. *Brasseur and S.Solomon (2005)*).

$$N = \sqrt{\frac{g}{T} \left(\frac{dT}{dz} - \Gamma \right)} \quad (2.5)$$

After their generation gravity waves can propagate vertically and horizontally, with vertical wavelengths of 5 to 15 km and horizontal wavelengths of 10 up to several 100 km. The wave period reaches from some minutes to several hours.

Whereby the buoyancy period $\frac{1}{N}$ is the minimum period and the coriolis period $\frac{1}{f}$ the maximum period. The coriolis parameter f is defined in equation 2.6 and depends on the latitude.

$$f = 2\Omega \sin(\Phi) \quad (2.6)$$

Here Ω is the rotational frequency of the earth and Φ is the latitude. Gravity waves transport energy and momentum, which are released when the waves break. They cause fluctuations in temperature, density, pressure and wind.

The main tropospheric sources of gravity waves are orography, convection and geostrophic adjustment, which includes baroclinic instabilities, jetstreams and frontogenesis. The generation by orography works by lifting of stable stratified layers due to an overflow of a mountain. Also gravity waves can be generated by an overflow of 'convection cells'. Moreover those 'convection cells' may press stable stratified layers in the upper troposphere together, so that the compression excites new gravity waves.

Another generation mechanism is the geostrophic adjustment. It can be imagined as follows: the initial situation is an unbalanced flow, which can be accompanied by e.g. baroclinic instabilities. Hereon the flow relaxes to a new balance state by redistribution of energy, momentum und vorticity. The excessive energy is then stratified as gravity waves.

In higher regions of the atmosphere gravity waves are mainly generated by wave-wave interactions (*Lossow (2003)*).

To describe a gravity wave mathematically, the fundamental fluid equations are needed as follows:

- momentum conservation

$$\frac{du}{dt} - fv + \frac{1}{\rho} \frac{\partial p}{\partial x} = X \quad (2.7)$$

$$\frac{dv}{dt} + fu + \frac{1}{\rho} \frac{\partial p}{\partial y} = Y \quad (2.8)$$

$$\frac{dw}{dt} + g + \frac{1}{\rho} \frac{\partial p}{\partial z} = 0 \quad (2.9)$$

- mass conservation

$$\frac{1}{\rho} \frac{d\rho}{dt} + \frac{\partial u}{\partial x} + \frac{\partial v}{\partial y} + \frac{\partial w}{\partial z} = 0 \quad (2.10)$$

- energy conservation

$$\frac{d\Theta}{dt} = Q \quad (2.11)$$

- with Θ as potential temperature:

$$\Theta = \frac{p}{\rho R} \left(\frac{p_0}{p} \right)^\kappa \quad (2.12)$$

Where (u,v,w) is the wind velocity vector, X,Y and Q are unspecified forcings, $\kappa = \frac{c_p}{c_v}$ and R is the ideal gas constant.

Those equations describe a coupled system of non-linear differential equations. For simplification the unforced case and a constant gravity acceleration are assumed. The equations are linearized by the perturbation approach. Here the quantities u,v,w,ρ and p are parted in a mean value and a perturbation from it. So u,v,w,ρ and p are defined as follows: $u = \bar{u} + u'$, $v = \bar{v} + v'$, $w = \bar{w} + w'$, $\rho = \bar{\rho} + \rho'$ and $p = \bar{p} + p'$. It is assumed, that the vertical mean velocity \bar{w} is zero. The density and the pressure only change with the height. Furthermore the WKB-approach is applied, which means that it is assumed, that \bar{u} , \bar{v} and N vary slowly over a wave cycle in the vertical. So that the derivative of \bar{u} , \bar{v} and N with respect to the time becomes zero. The differential equation system is solved with the simple wave approach:

$$(u', v', w', \frac{\Theta'}{\Theta}, \frac{p'}{\bar{p}}, \frac{\rho'}{\bar{\rho}}) = (\tilde{u}, \tilde{v}, \tilde{w}, \tilde{\Theta}, \tilde{p}, \tilde{\rho}) * \exp[i(kx + ly + mz - \omega t) + \frac{z}{2H}] \quad (2.13)$$

Rearranging and factoring out the soundwaves, by assuming incompressibility results in the dispersion relation (*Fritts and Alexander (2003)*):

$$\hat{\omega}^2 = \frac{N^2(k^2 + l^2) + f^2(m^2 + \frac{1}{4H^2})}{k^2 + l^2 + m^2 + \frac{1}{4H^2}} \quad (2.14)$$

Where $\hat{\omega} = \omega - k\bar{u} - l\bar{v}$ is the intrinsic frequency, which would be observed in a frame of reference moving with the background wind. k,l,m are the wavenumbers. For vertically propagating gravity waves k,l,m are real. With ω the phase velocity

c and the group velocity c_g and accordingly the intrinsic phase and group velocities (\hat{c} , \hat{c}_g) can be determined. The phase velocity indicates the propagation direction of the wave and the group velocity indicates the propagation of momentum and energy transport.

$$c = (c_x, c_y, c_z) = \left(\frac{\omega}{k}, \frac{\omega}{l}, \frac{\omega}{m} \right) \quad \hat{c} = (\hat{c}_x, \hat{c}_y, \hat{c}_z) = \left(\frac{\hat{\omega}}{k}, \frac{\hat{\omega}}{l}, \frac{\hat{\omega}}{m} \right) \quad (2.15)$$

$$(c_{gx}, c_{gy}, c_{gz}) = \left(\frac{\partial \omega}{\partial k}, \frac{\partial \omega}{\partial l}, \frac{\partial \omega}{\partial m} \right) \quad (\hat{c}_{gx}, \hat{c}_{gy}, \hat{c}_{gz}) = \left(\frac{\partial \hat{\omega}}{\partial k}, \frac{\partial \hat{\omega}}{\partial l}, \frac{\partial \hat{\omega}}{\partial m} \right) \quad (2.16)$$

As mentioned above, gravity waves can propagate vertically and horizontally. If a wave propagates vertically without any damping, its amplitude increases with ascending height, due to the descending air density. At a critical height the amplitude becomes so large, that the wave becomes unstable and breaks. Also gravity waves break when the horizontal phase velocity becomes equal to the zonal background wind. Then the vertical wavenumber tends to infinity and the vertical wavelength approaches zero. The wave cannot propagate vertically anymore.

Since the zonal background wind is in winter positive and in summer mainly negative. The latter breaking criterium results an annual variation of waves with dominating negative phase velocities in winter time and dominating positive phase velocities in summer time (see fig. 3).

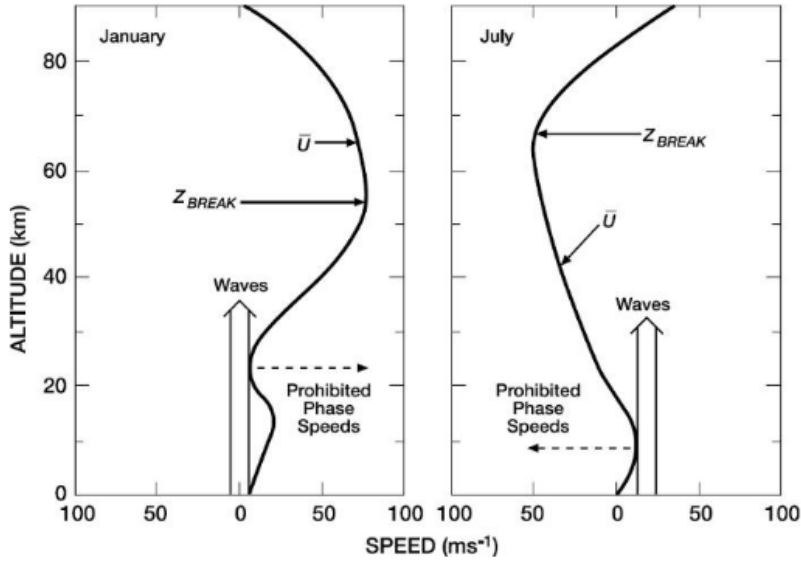


Figure 3: Typical vertical zonal mean wind profiles for winter (left) and summer (right). Gravity waves are filtered, when their phase velocities are equal the backgroundwind \bar{u} . z_{break} marks the lower boundary of the gravity wave breaking level (*Brasseur and S.Solomon (2005)*, based on *Lindzen (1981)*)

2.3 Planetary waves

Planetary waves distinguishes from gravity waves in their restoring force, the Coriolis force. They are called 'planetary waves' due to their global scales with horizontal wavelengths of 1.000 to 10.000 km and periods of 1 to 30 days. Orographic obstacles, land-sea contrasts or adiabatic processes can excite planetary waves. As gravity waves, planetary waves propagate horizontally and vertically. In doing so they transport energy and momentum, which are transferred when the waves break. Due to the large scales of the planetary waves, the Coriolis force has a big influence on them. While describing the oscillations of planetary waves with an air parcel, the Coriolis force has to be taken into account. Thus the absolute velocity (\vec{u}_a) of an air parcel in the inertial system is composed of the relative velocity (\vec{u}_r)

and the motion by the earth rotation (\vec{u}_e).

$$\vec{u}_a = \vec{u}_r + \vec{u}_e \quad (2.17)$$

The rotation of the velocities delivers:

$$\vec{\nabla} \times \vec{u}_a = \vec{\nabla} \times \vec{u}_r + \vec{\nabla} \times \vec{u}_e \quad (2.18)$$

Inserting $\vec{u}_e = \Omega \times \vec{r}$ with Ω as the angular velocity of the earth obtains:

$$\vec{\nabla} \times \vec{u}_a = \underbrace{\vec{\nabla} \times \vec{u}_r}_{\zeta} + \underbrace{\vec{\nabla} \times \vec{\Omega} \times \vec{r}}_{f=2\vec{\Omega} \cdot \sin\Phi} \quad (2.19)$$

The rotation of the velocity is also called vorticity. In equation 2.19 the lefthand side represents the absolute vorticity, the second term the relative vorticity ζ and the third term the planetary vorticity f . The planetary vorticity is the latitudinal related Coriolis parameter f . For horizontal flows the absolute vorticity is conserved in a barotropic and frictionless atmosphere with constant height (*Mager (2004)*).

$$\frac{D_h \zeta + f}{Dt} = \frac{D \left(\frac{\partial v}{\partial x} + 2\vec{\Omega} \cdot \sin\Phi \right)}{Dt} = 0 \quad (2.20)$$

However due to e.g. orography or high and low pressure areas the height of the atmosphere is not constant. In this case the potential vorticity q is conserved. The potential vorticity considers the relation from the absolute vorticity to the height of the rotating column.

$$q \equiv -g \frac{\partial \Theta}{\partial p} (\zeta + f) \quad (2.21)$$

Equation 2.21 represents the potential vorticity in isentropic coordinates, where Θ is the potential temperature.

So planetary waves are generated due to the conservation of the vorticity by latitudinal variation of the Coriolis force. The description of the spatial variation of the Coriolis parameter in cartesian coordinates succeeded *Rossby (1939)* using the so called beta-plane. That is why planetary waves are also called Rossby waves. Here the Coriolis parameter f is expanded in a Taylor series around the point y_0 .

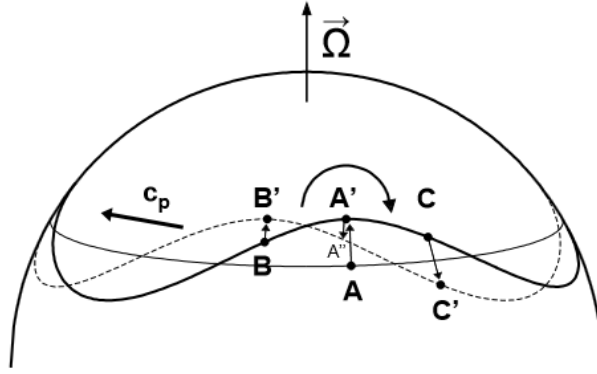


Figure 4: Schematic generation of a planetary wave. A planetary wave is generated due to the conservation of the vorticity by the latitudinal variation of the Coriolis force. c_p is the phase velocity of the westwards propagating wave (*Mager (2004)*).

The series is truncated after the linear term. So we obtain:

$$f(y) = f_0 + \beta \cdot y \quad (2.22)$$

with $\beta = \frac{2 \cdot \Omega \cos(y_0)}{R}$ is the linear coefficient, where R is the earth radius.

There are four types of planetary waves: transient, stationary, standing waves and oscillations.

- If the phase changes with respect to the longitude it is spoken of transient waves. Those waves have a nonzero wavenumber s and frequency ω and can propagate eastward as well as westward.
- A planetary wave is called stationary if it is stationary with respect to the longitude. Here the frequency ω is zero but the wavenumber s is nonzero.
- A standing planetary wave is generated, if two equal transient planetary waves superpose. The transient planetary waves have to propagate in opposite direction and possess equal wavenumbers ($s_1 = s_2$) and frequencies ($\omega_1 = \omega_2$).

- The special case oscillation exists if it oscillates in time with the same phase at all longitudes. Here the frequency ω is nonzero but the wavenumber s is zero. The oscillation moves with respect to the latitude.

In figure 4 the schematic generation of planetary waves is shown. Imagine 3 air parcels, located on the same latitude line next to each other in the northern hemisphere (positions: B,A,C). In the resting position the relative velocity and the planetary vorticity are zero. If the air parcel of the position A is moved northwards to higher latitudes (position A') the planetary vorticity increases. Because the absolute vorticity has to be conserved, the relative vorticity has to become negative. Consequently it arises an anti cyclonic flow around A. This flow induces a southward motion of the air parcel in Position C to C' and a northward motion of the air parcel in position B to B'. The deflections from the air parcel of position B and C resulting again in cyclonic ($\zeta > 0$) or anti cyclonic ($\zeta < 0$) flows.

With the potential vorticity as a conserved quantity following the flow, the linear wave approach and the assumption that the zonal wind \bar{u} is constant we obtain the dispersion relation for planetary waves (Matthias (2013)):

$$\omega = c \cdot k = \frac{ku - \beta k}{k^2 + l^2 + \left(\frac{f^2}{N^2}\right) \left(m^2 + \frac{1}{4H^2}\right)} \quad (2.23)$$

The zonal wind field where a planetary wave can vertically propagate is limited. The conditions for the vertical propagation are given by the Charney- Drazien criterion (Charney and Drazien (1961)):

$$0 < \bar{u} - c < u_{crit} \equiv \frac{\beta}{k^2 + l^2 + \frac{f^2}{N^2 4H^2}} \quad (2.24)$$

According to equation 2.24 \bar{u} has to be positiv, but not to large. Thus planetary waves only can propagate vertically during moderate eastward winds. The critical velocity u_{crit} which represents the upper limit for \bar{u} is related to the zonal and meridional wavenumbers with indirect proportionality. Furthermore equation 2.23 reveals that the difference between $\bar{u} - c$ has to be larger than zero and that a planetary wave can only propagate westward relative to the background wind. Otherwise the wave dissipates. Since the zonal wind is eastward in winter and

westward in summer in the stratosphere, planetary waves can only propagate from the troposphere into the mesosphere during winter. However, planetary waves are generated in-situ in the summer mesosphere (e.g. *Matthias (2014), Holton and Alexander (2000)*).

2.4 Atmospheric tides

Next to gravity and planetary waves there is another wavetype which is important for the MLT dynamics: the atmospheric tides. Atmospheric tides are global scale oscillations of temperature, wind, pressure and density. They are primarily excited by the periodic absorption of solar radiation by trace gases in the troposphere and stratosphere. The infrared proportion of the solar spectrum is absorbed by tropospheric water vapor. Stratospheric ozone absorbs UV radiation. Molecular oxygen and molecular nitrogen absorb EUV and UV radiation in lower thermospheric heights. The heating rates, which are related to the diurnal variation of the radiation absorption, can be Fourier decomposed into subharmonics of a solar day. So typically periods of atmospheric tides are e.g. 24, 12 and 8 hours. Whereby the 24 hour tide is mainly generated in the troposphere and the 12 hour tide is mainly generated in the stratosphere.

In figure 5 the schematic of vertical variations of tidal heating is shown. Note that at heights of 80 to 100 km no radiation is absorbed, which means no excitation of atmospheric tides takes place. Nevertheless the dynamics in those height regions are strongly influenced by the tides. This is because they are able to propagate vertically and with increasing heights, the amplitudes of the tides increase also due to the decreasing density. So they have very large amplitudes at mesospheric heights, where they interact with other waves.

There are two types of solar atmospheric tides: the migrating and the non-migrating solar tides. The migrating tides are sun synchronous. While they propagate westward, they can be erased by strong eastward winds or amplified by westward winds. Then there are the non-migrating tides, which are not sun synchronous. They can propagate west- and eastward at a different speed to the sun. Differences in the topography with longitude, land-sea contrasts, surface interactions or the latent heat release due to the deep convection in the tropics can

cause the generation of non-migrating tides (*Forbes (1995), Forbes (1982)*).

Atmospheric tides can also be excited by time variations in gravitational forcing induced by the moon. Those kind of tides are much weaker than the solar tides, which are the dominating waves in the mesosphere with amplitudes of up to 50 m/s. However there are recent publications, which verify that the semidiurnal lunar tide has a maximum peak during SSWs (*Chau et al. (2015)*).

To describe the latitudinal and temporal structures of the tides, we have to start with the primitive equations (see equations 2.7-2.11, excluding 2.9 since just the horizontally momentum equations are needed). Those are linearized and the perturbation approach is applied. To solve this set of equations for tides, the separation approach is used, which looks as follows:

$$\begin{aligned}\Phi'(\phi, \lambda, z, t) &= \hat{\Phi}(\phi, z) \cdot e^{i(s\lambda - \sigma t)} \\ \hat{\Phi}(\phi, z) &= \sum \Theta_n(\phi) G_n(z)\end{aligned}\tag{2.25}$$

Where ϕ is the latitude, λ the geographic longitude, z is the altitude, t is the time, s the zonal wavenumber and σ is the frequency. This example is for the separation of z . It is processed similarly for the separation of t . After the application of the separation approach we yield the so called 'Laplace's tidal equation', which describes the latitudinal and temporal structures of the tides (e.g. *Longuet-Higgins (1968), Andrews et al. (1989)*):

$$L\Theta_n + \epsilon_n\Theta_n = 0\tag{2.26}$$

With L as Laplace operator:

$$L = \frac{\partial}{\partial \mu} \left[\frac{(1 - \mu^2)}{(\eta^2 - \mu^2)} \frac{\partial}{\partial \mu} \right] - \frac{1}{\eta^2 - \mu^2} \left[-\frac{s(\eta^2 + \mu^2)}{\eta(\eta^2 - \mu^2)} + \frac{s^2}{1 - \mu^2} \right]\tag{2.27}$$

where $\mu = \sin\phi$ and $\eta = \sigma/(2\Omega)$. $\epsilon_n = (2\Omega a)^2/gh_n$ are the eigenvalues and Θ_n the eigenfunctions, called Hough functions, to the atmospheric tides, which are eigen oscillations of the earth atmosphere. Where a is the earth radius, g the earth acceleration and h_n is the equivalent depth, which couples the latitudinal structure of the tides with their vertical structure.

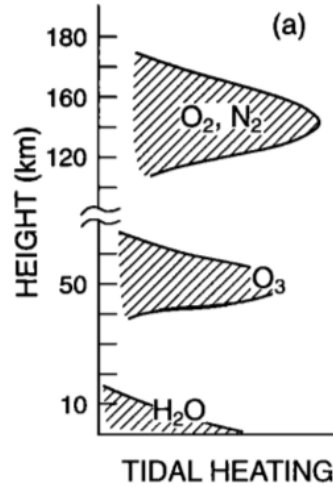


Figure 5: Vertical variation of tidal heating. The heating maxima in troposphere, stratosphere and lower thermosphere are caused by maximal absorption of various parts of the solar spectrum due to water vapor, ozone, molecular oxygen and molecular nitrogen (*Forbes (1995)*)

2.5 Sudden stratospheric warming (SSW)

On the 30th of January 1952 *Scherhag (1952)* observed a sudden and short-termed increase of temperature and a zonal wind reversal in the stratosphere at the same time. In figure 6 the temperature gradient between 60°N and 90°N and zonal mean zonal wind at 10 hPa during a major SSW event is shown. One can clearly see the sudden increase of the temperature gradient around the 20th day of the year 2009. At the 23th day the temperature gradient reaches its maximum and the wind reverses from positive to negative, which is characteristic for a major event. The phenomenon of the sudden stratospheric warming, short SSW, bases, according to *Matsuno (1971)*, upon vertically propagating planetary waves and their interactions with the zonal background wind. As mentioned before, planetary waves can propagate in the stratosphere only during eastward background winds thus SSWs occur only in winter (*Charney and Drazin (1961)*).

If a planetary wave breaks, due to reaching the critical level u_{krit} or to large amplitudes, its energy and momentum are transposed to the atmosphere and background wind. It follows a heating and a westward acceleration respectively deceleration

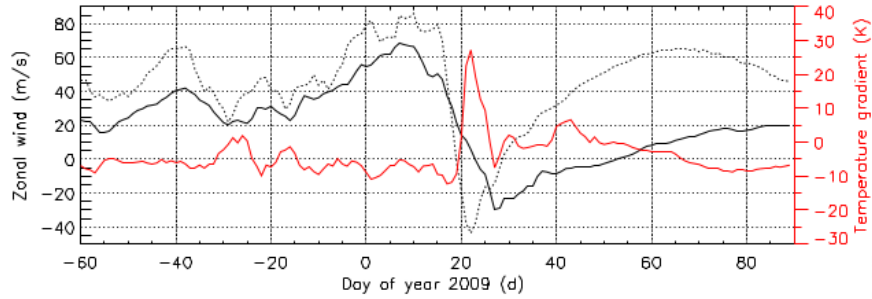


Figure 6: Temperature gradient in 10 hPa (red solid line), zonal mean zonal wind in 10 hPa (black solid line) and zonal mean zonal wind in 1 hPa (black dashed line) for the winter 2008/2009 between 60°N and 90°N , based on MERRA data. The onset day of the major SSW event is identified on the 23.01.2009, where the temperature gradient peaks and the mean zonal mean wind in 10 hPa becomes negative.

of the background wind. In the case of a SSW the westerly polarjet is weakened or even reversed resulting in easterly winds. As a consequence the polar vortex deforms or even bursts. This enables warm air to enter the polar region, which is usually encircled by the polarjet. A sudden increase of temperature in the stratosphere in higher latitudes is observed.

According to *Labitzke and Naujokat* (2000) SSWs can be classified into 4 types. The minor, major, final and Canadian SSW.

- It is spoken of a minor warming, if the temperature gradient in the stratosphere is increased. Moreover intense minor warmings can result in a reversal of the temperature gradient. They are identified by a minimum of the zonal mean wind at 10 hPa and in uncertain cases also at 1 hPa. But note, that minor warmings don't cause a wind reversal and a total change of the circulation at heights of 10 hPa. Latter one is a main characteristic of a major warming event.
- Major warmings occur mostly in the mid winter. They are associated with a warming of the north polar region, a reversal of the meridional temperature gradient and a breakdown or splitting of the polar vortex (see fig. 7). They can be identified by a zonal wind reversal at 60°N at heights of 10 hPa and a temperatur gradient maximum between 60°N and 90°N at 10 hPa.

- Then there are the Canadian Warmings, which mostly occur in November and December. The intensification and northward displacement of the Aleutian high over Canada can result in a briefly reversal of the meridional temperature gradient and the zonal mean winds. But this doesn't lead to a breakdown of the polar vortex, as it is the case during a Major Warming.
- Last but not least there are the Final Warmings. They occur every year in spring with the prolonged semi annual zonal wind reversal. Over summertime the prevailing zonal winds are westward and over wintertime eastward directed.

Due to the wind reversal during the SSWs the vertical propagation of gravity waves is influenced. During winter westward propagating gravity waves dominate. Those waves drive the residual circulation and cause the warm winter mesosphere. In case of a wind reversal, due to a SSW event, those waves are filtered. Now gravity waves with positive phase velocities dominate and influence the residual circulation from the summer to the winter pole. Air masses are transported equatorwards and it follows an adiabatic cooling of the winter mesosphere. So during a SSW not only the stratospheric temperatures increase but also the temperatures in the mesosphere decrease (*Matthias (2014), Körnich and Becker (2010)*). Furthermore the gravity wave activity is related to the position of the polar vortex. This is subject of the discussion by *Wang and Alexander (2009)*.

SSWs are mainly observed in the northern hemisphere, since the polar vortex cannot establish very well due to the increased planetary wave activity. In the southern hemisphere there are much less distracting landmasses and much less planetary waves. So the polar vortex over the south pole is more stable. Nevertheless, there are also SSWs observed in the southern hemisphere, as it is described e.g. by *Venkat Ratnam et al. (2004)*, but with a much lower frequency as compared to the northern mesosphere.

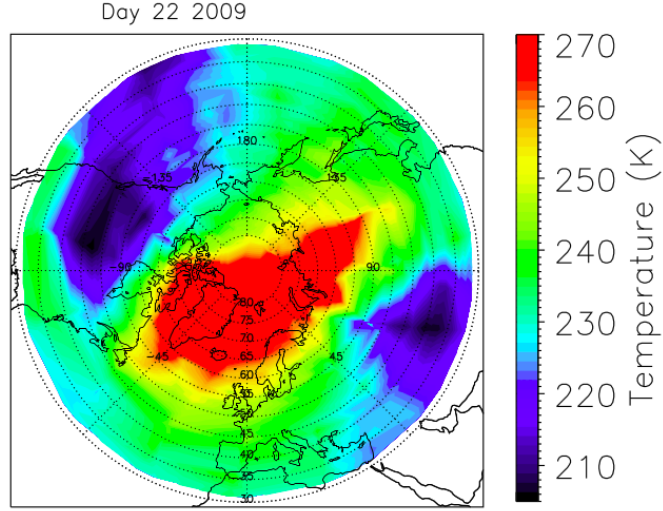


Figure 7: Split polar vortex in the northern hemisphere during the SSW onset in 2009 (courtesy of V. Matthias)

3 Instruments and data

3.1 Basic principles of the radar technology

The measuring instrument *radar* (radio detection and ranging) is based on linear and constant propagation and reflection of electromagnetic waves with a frequency range from 1 kHz to 3 GHz. Electromagnetic waves propagate with speed of light and are reflected on irregularities of the refraction index of the atmosphere. Changes of the refraction index can be caused by free electrons, water vapor and temperature changes. This relation is described with equation 3.1 (e.g. *Sato*).

$$n^2 = 1 + \frac{0.375 \cdot p_{H_2O}}{T^2} + \frac{7.76 \cdot 10^5 \cdot p_{atmosph}}{T} + \frac{N_e}{2N_c} \quad (3.1)$$

Where p_{H_2O} is the water vapor partial pressure, T is the temperature, $p_{atmosph}$ is the atmospheric pressure, N_e is the electron density and N_c is the critical plasma density, at which total reflection takes place. In the troposphere the refraction index is strongly related to variations of the water vapor partial pressure. Variations in the temperature distribution are relevant at lower stratospheric heights. From 50 km upwards the electron density becomes steadily an more important role for

irregularities of the refraction index.

The signal of the reflected wave can be detected by a receiver. By the propagation time of the signal the distance of the backscatterers can be determined as follows (e.g. *Richards*):

$$L = \frac{c \cdot t}{2} \quad (3.2)$$

Here is L the distance between the radar and the backscatterer, c the speed of light and t the measured propagation time. With the radar equation (equation 3.3) it is possible to calculate the power of the backscattered signal. Since electromagnetic waves are mostly just partially reflected, a part of the signal continues propagating. Thus the power of the back scattered signal is weaker than the power of the emitted signal (e.g. *Skolnik*).

$$P_r = \frac{P_t \cdot G^2 \cdot \lambda^2 \cdot \sigma}{(4\pi)^3 \cdot R^4} \quad (3.3)$$

Where P_r is the power of the received signal, P_t is the power of the transmitted signal, λ is the wavelength and G is the antenna gain, which is areadependent.

If the backscatterer is moving the reflected signal is Doppler shifted. The Doppler shift provides the radial velocity of the backscatterer. For the calculation of the accurate height of the backscatterer swing angle and propagation time have to be considered. Since the height resolution is technically limited, amplitude and phase of every signal are assigned to a height gate. Subsequently it is averaged over every height gate.

3.2 The meteor radar

If a meteoroid passes the atmosphere, it is decelerate by air molecules and heats up. At a critical temperature the components of the meteoroid evaporate and a plasma is forming around the meteoroid. The luminous plasma is called meteor. Behind the meteor an ionization trail develops. This ionization trail has a very low density and so it is moved with the neutral wind. Typical ablation heights of meteors are from 80 to 100 km (*Stober (2009)*). With the meteor radar it is possible to determine the radial drift velocity of the ionization trail of a meteor from the Doppler shift. In this thesis the gravity wave momentum flux in the mesosphere is determined and analyzed in relation to sudden stratospheric warmings. The

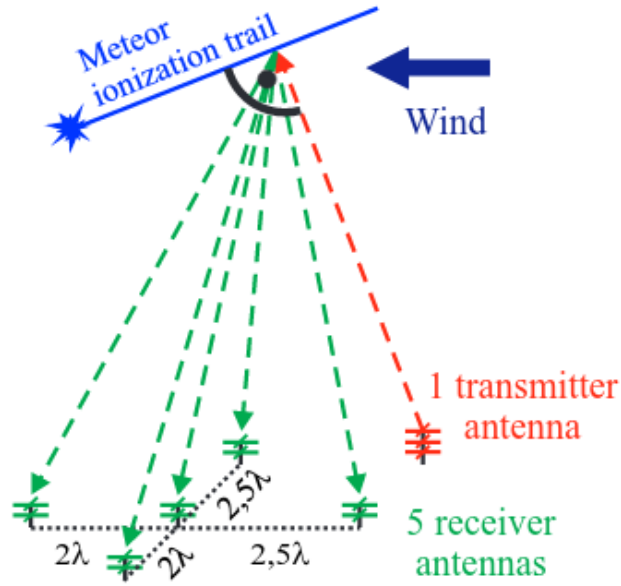


Figure 8: Setup of a SKiYMET meteor radar, where λ is the wavelength of the transmitted signal (*Placke (2014)*).

momentum flux is calculated by fluctuations in the mesospheric wind field, which is determined by all sky-interferometric (SKiYMET) meteor radar data.

The meteor radar consists of one transmitting antenna and five receiving antennas. The latter are arranged in an asymmetric cross to minimize biases of the phases and following errors in the meteor location (*Hocking (2005)*). The transmitting antenna emits circumpolar electromagnetic waves, which are reflected at ionization trails. The meteor radar just receives signals, which are reflected at the scatterers with an angle of 90° . The meteor echos are then received by the five receiving antennas and interferometric analyzed, so that time, location, echo amplitude and radial velocity for every meteor event can be determined (*Mager (2004)*).

The here used meteor radars are located in Andenes ($69.27^\circ N, 16.04^\circ E$) and in Juliusruh ($54.63^\circ N, 13.37^\circ E$). Continuous measurements are performed in Andenes from October 2001 and in Juliusruh from May 2007. Both radars have a transmission frequency of 32.55 MHz and a peak power of 12 kW. Till 2014 the pulse code was in Andenes and Juliusruh of the type mono. The range resolution was for both radars 2 km and the pulse repetition frequency (PRF) was in An-

3.4 Wind fitting

The determined wind field from 78 km to 100 km is composed of the background-wind, planetary waves, tides and gravity waves. For the calculation of the gravity wave momentum flux the gravity wave part of the wind field has to be extracted. This is very challenging, because the most gravity waves are very small scaled and hard to predict due to their diverse sources. To obtain the gravity wave part of the windfield, the wind including backgroundwind, planetary waves and tides is fitted. Subsequently the fit is subtracted from the measured wind. It is assumed, that the residuum of this subtraction represents the gravity waves activity. The equation for the wind fit is shown in equation 3.6.

$$u_{fit}, v_{fit} = u_0, v_0 + \sum_{i=8,12,24} A_i \cos(\omega_i t + \Phi_i), \quad w_{fit} = w_0 \quad (3.6)$$

Here u_0, v_0 are the horizontal mean winds, averaged over 24 hours. They represent the background wind and planetary waves (for further explanations, see below). The second term represents the terdiurnal, semidiurnal and diurnal tides with A for the Amplitudes, ω for the frequencies and Φ for the phases. The vertical wind component w is just fitted with the vertical mean wind, averaged over 24 hours, because the tides in the vertical component are with their single-digit velocities neglectable small.

The wind is fitted by the method of the adaptive spectral filtering. This means, that every tide has its own fitting window, which is adaptive to the period of the several tide. Following the terdiurnal tide has a fitting window of $8h \pm 4h$, the semidiurnal tide has a fitting window of $12h \pm 6h$ and the fitting window of the diurnal tide ranges over $24h \pm 12h$.

In the beginning of the fit the backgroundwind is fitted. This is done by a 24 hour average. Since in wintertime the 10-day and 16-day planetary waves dominates, the variations of the wind over 24 hours due to planetary waves are very small compared to the values of the 24 hour averaged wind. Therefore the 24 hour average not only represents the background wind, in addition it contains the planetary wave part also.

After the background wind is fitted, it is subtracted from the measured wind. It

follows the fit of the diurnal tide by the residual of the measured and the background wind. Subsequently the diurnal tide fit is removed from the residual and the procedure is reiterated for the semidiurnal and terdiurnal tides.

Eventually the adaptive spectral filtering method is continued in 1 hour steps over the entire period, which has to be fitted.

In the first panel of figure 9 the measured zonal wind from 20.01.2009 to 22.01.2009 is shown. The measurement was taken in Juliusruh. In the second panel the fitted zonal wind for the same period is shown. The measured and the fitted wind matches quite well. But there are still some differences, e.g. during the first half of 21.01.2009 from 82 km to 98 km or during the second half of the 23.01.2009 from 86 km to 98 km. In the third panel the residual of the measured and fitted zonal wind is shown. It is anticipated that the residual of the measured and fitted wind represents fluctuations due to gravity wave activity. Following, in this case the strongest gravity wave activity occurs during the second half of 22.01.2009 from 89 km to 99 km.

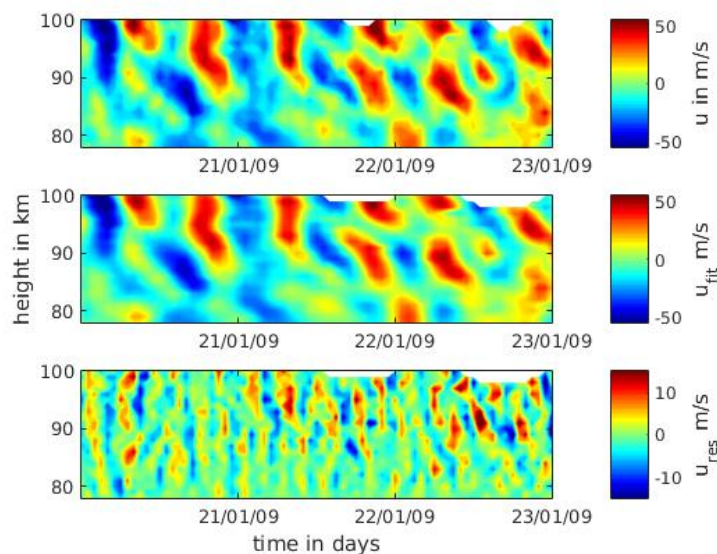


Figure 9: In the upper panel is the zonal wind, in the middle panel the fitted zonal wind and in the lower panel the resulting residual zonal wind. The residual zonal wind is representative for fluctuations, caused by gravity waves.

3.5 Calculation of the gravity wave momentum flux

The momentum flux of the gravity waves is determined by a method, which is presented by *Hocking et al.* (2001). Here the dual-beam formulation introduced by *Vincent and Reid* (1983) is generalized, so that the traditional dual-beam is a special case. The deviations between the measured radial velocity v_{rad} and the fitted radial velocity v_{rad_m} are assumed to represent the true wind variability v'_{rad} , due to gravity waves. Then the quantity Λ is minimized by a least square fit in equation 3.7 to ensure a good fit of the variability.

$$\Lambda = \sum ((v'_{rad})^2 - (v'_{rad_m})^2)^2 \quad (3.7)$$

The summation is over all detected meteor positions within the oversampled 1 km and 1 hour time intervals. $v'_{rad} = v_{rad} - v_{rad_m}$ and v'_{rad_m} is the fitted variability, which is shown in equation 3.8.

$$v'_{rad_m} = u' \sin\Theta \cos\Phi + v' \sin\Theta \sin\Phi + w' \cos\Theta \quad (3.8)$$

Inserting equation 3.8 into equation 3.7 yields:

$$\begin{aligned} \Lambda = \sum [& (v'_{rad})^2 - u'^2 \sin^2\Theta \cos^2\Phi + v'^2 \sin^2\Theta \sin^2\Phi + w'^2 \cos^2\Theta \\ & + 2u'v' \sin^2\Theta \cos\Phi \sin\Phi + 2u'w' \sin\Theta \cos\Theta \cos\Phi \\ & + 2v'w' \sin\Theta \cos\Theta \sin\Phi]^2 \end{aligned} \quad (3.9)$$

Subsequently Λ is partially differentiate with respect to $u'^2, v'^2, w'^2, u'v', u'w', v'w'$ and setted to zero. After some rearranging this delivers a matrix equation system which produces estimations for $\overline{u'^2}, \overline{v'^2}, \overline{w'^2}, \overline{u'v'}, \overline{u'w'}, \overline{v'w'}$ as it is shown in the Appendix (equation 7.1).

3.6 Parameter variations

3.6.1 Number of meteors

For the momentum flux calculation there has to be a minimum amount of meteors per height and time bin. This minimum amount is user specified. If the amount is too small the calculated momentum flux can be distorted due to outliers. In the case of a too large specified amount of meteors it may occur too many NaNs. To verify what is an appropriate amount of meteors the momentum flux was calculated with 3 different specified meteor amounts (30, 45 and 60). In the figures 10-12 the respectively momentum fluxes are shown for the period ± 30 days around the SSW onset in 2006 (20.01.2006). First of all, the 3 figures seem to be quite similar. But still there exist some differences which should be noted.

The momentum flux in figure 10 shows the largest values of the 3 figures. This one was calculated by 30 meteors per time and height bin. Those larger values can be observed e.g. from the central day to day +20 from 80 km to 84 km or from day +20 to day +30 from 84 km to 94 km. The stronger values could be explained by the small minimum amount of meteors. So outliers can falsify the calculated momentum flux stronger.

Another difference, which can probably also be attributed to outliers, is the momentum flux from the central day to day +5 at heights from 96 km to 98 km. In figure 10 the momentum flux during this period and in this region is negative. In figure 11, which shows the momentum flux calculated by 45 meteors per time and height bin, the momentum flux in the same period and height region is positive. In figure 12, which shows the momentum flux calculated by 60 meteors per time and height bin, the observed momentum flux is positive also.

Eventually the minimum amount of 30 meteors is disregarded because it is not reliable, due to the too small amount of meteors.

The momentum flux in figure 11 shows in general larger values than in figure 12, since it is calculated with a smaller minimum amount of meteors. However, in figure 12 more NaNs occur than in figure 11, because the minimum amount of meteors was too large.

So in conclusion, 45 meteors are introduced as minimum meteor amount. It delivers more reliable results than 30 and less NaNs than 60 for the minimum amount of meteors.

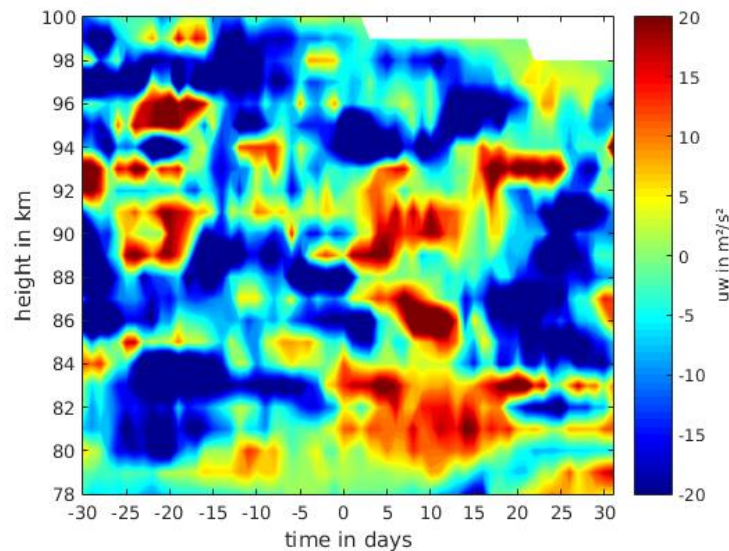


Figure 10: Momentum flux calculated with a minimum meteor event amount of 30. The central day is the 20.01.2006.

3.6.2 Averaging windows and steps

With the Hocking method, which is introduced in chapter 3.5, the momentum flux can be calculated per time and height bin. If the variation of the momentum flux is considered over a longer time period e.g., two months or one year, it is recommended to average the calculated hourly momentum flux values over a longer time window. The difficulty here is to determine an appropriate averaging window and corresponding shifting steps.

According to the Nyquist sampling theorem, the maximum shifting step is half the length of the averaging window. Otherwise the averaged momentum flux is falsified. So in case of a 20 days averaging window, it is recommended to choose a time shift of not more than 10 days. Moreover averaging window and shifting step should be chosen in consideration of the observed time period and scales.

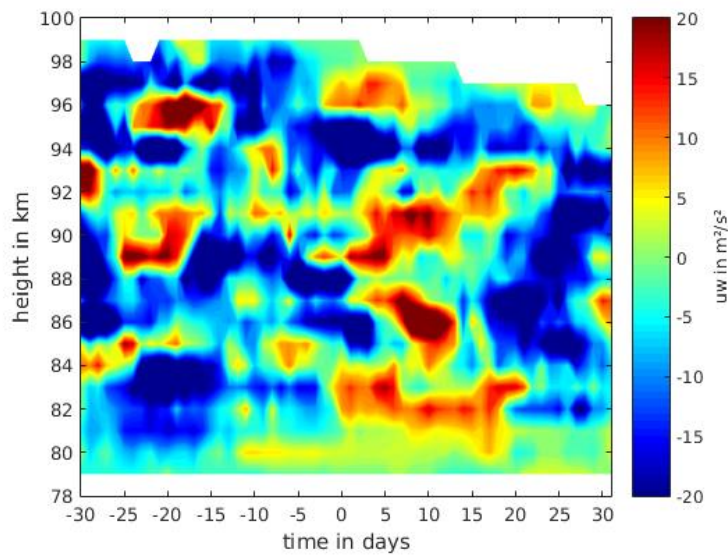


Figure 11: Momentum flux calculated with a minimum meteor event amount of 45. The central day is the 20.01.2006.

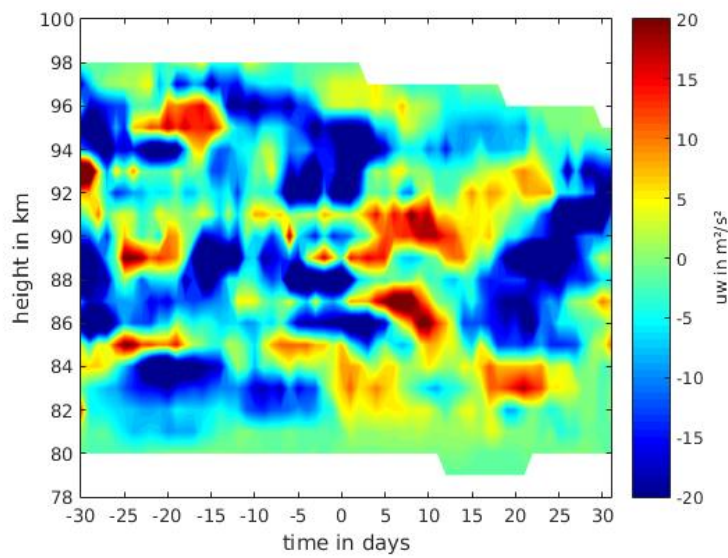


Figure 12: Momentum flux calculated with a minimum meteor event amount of 60. The central day is the 20.01.2006.

The SSW event occurs sudden and lasts just over a couple of days. Accordingly the shifting step should not be selected to big, for the analysis of the momentum flux during a SSW event. Whereas for the annual variation of the momentum fluxes it is advised, to select bigger shifting steps. So possible annual trends could be verified better.

In figure 13 and 14 the momentum flux for the time period ± 30 days around the 23.01.2009 is shown. The 23.01.2009 is chosen as the central day, because it is the SSW onset. Figure 13 shows the 10 day averaged momentum flux shifted by 1 day and figure 14 shows the 10 day averaged momentum flux shifted by 5 days. The trend of the momentum flux is in both figures similiar, whereas the 1 day moved avererage shows more details. Especially from day -25 to day -5 at the height region from 88 km to 94 km the structures are completely smoothed by the 5 day shifted average. Therefore in the following analyses, of the momentum flux for a time period of ± 30 days around the SSW onset, it is averaged over 10 days and shifted by 1 day.

In figure 15 and 16 the momentum flux for the time period from the 01.01.2009 to the 01.01.2010 is shown. Figure 15 shows the 20 day averaged momentum flux shifted by 5 days and figure 16 shows the 20 day averaged momentum flux shifted by 10 days. Figure 15 shows more details, due to the smaller shifting steps. This can be observed, e.g from day 90 to day 120 at heights from 92 km to 94 km or from day 150 day to day 210 at heights from 82 km to 87 km. However for the consideration of the annual variation of the GW momentum flux, it is more appropriate to use the large shifting steps. Thus large scaled characteristics of the annual variation are more obvious in smoothed than in detailed structures. So in the following analyses of the momentum flux for a time period of one year, it is averaged over 20 days and shifted by 10 days.

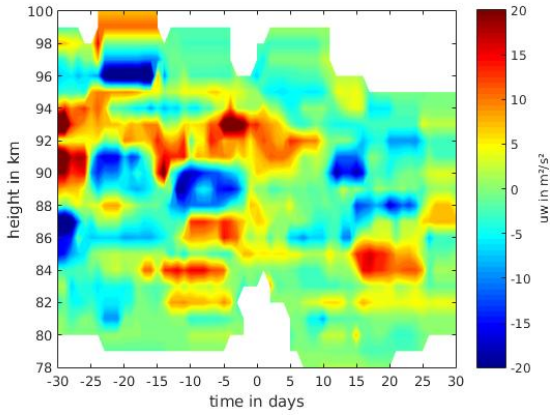


Figure 13: 10 day averaged momentum flux shifted by one day.
The central day is 23.01.2009.

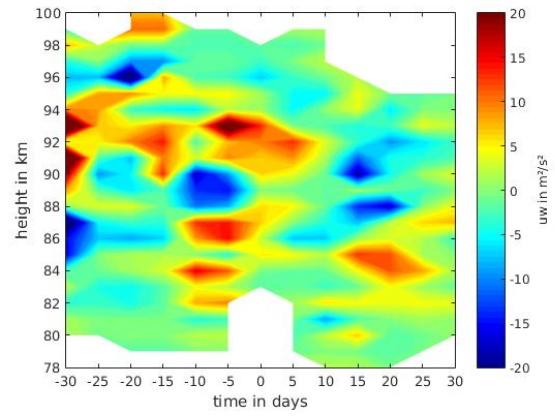


Figure 14: 10 day averaged momentum flux shifted by 5 days.
The central day is 23.01.2009.

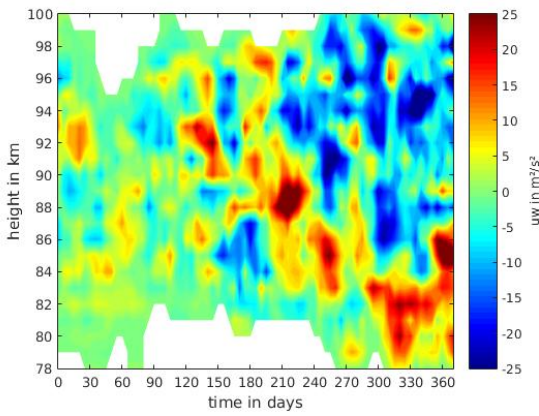


Figure 15: 20 day averaged momentum flux shifted by 5 days
from 01.01.2009 to 01.01.2010.

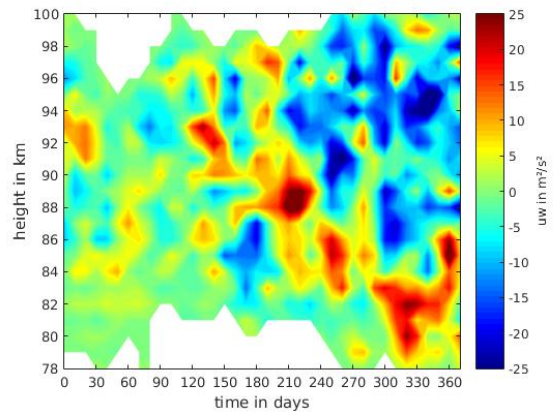


Figure 16: 20 day averaged momentum flux shifted by 10 days
from 01.01.2009 to 01.01.2010.

3.6.3 Weighting of the calculated momentum flux

As described in 3.6.2 the momentum flux is averaged over different time windows according to the considered time period. Here it is important to consider that NaNs can distort the average. To minimize that effect, the averaged values are weighted. For the weighting the number of NaNs per averaging window is taken into account and a weighting factor is calculated. This weighting factor varies from zero to one. If there is no NaN in an averaging window the weighting factor is one. In the case of a weighting factor equals zero, the average is setted to NaN. In figure 17 the nonweighted and in figure 18 the weighted averaged momentum flux is shown. The time period lasts over ± 30 days centered around the 23.01.2009. It was averaged over 10 days shifted by one day. Here it is obvious how strong NaNs can distort the average. In figure 17 the momentum flux is partly more as twice as strong than the weighted momentum flux in figure 18. This can be caused by too little meteor events or too high calculated momentum fluxes, due to outliers or technical problems of the radar. The latter one can be excluded since the zonal wind is determined without any distortions.

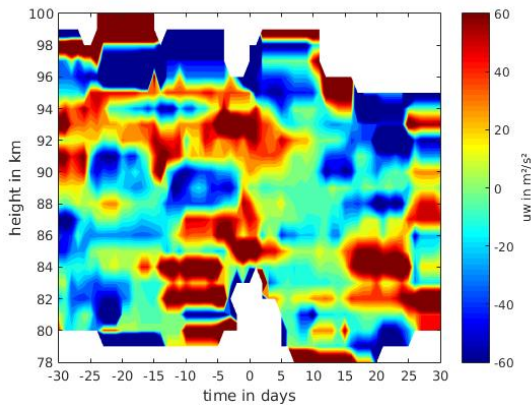


Figure 17: Averaged momentum flux with 23.01.2009 as central day.

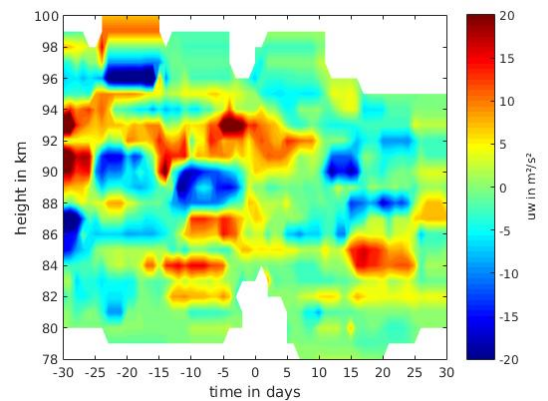


Figure 18: Weighted averaged momentum flux with 23.01.2009 as central day.

4 Measurements

4.1 Identification of a SSW

Before we start to investigate the momentum flux, we have to identify potential major SSW. In this thesis the onset day of a major SSW is defined by the zonal wind reversal at the 10 hPa level, based on *Labitzke and Naujokat (2000)*. In case of a major warming the wind reverses throughout the mesosphere. For the identification of a major SSW the mean zonal wind from November to April for every year is plotted and verified for the sudden and short term wind reversal from positive to negative directions (cf. fig. 6). Since the meteor radar provides data from the 0.01 hPa level upwards, it is recommended to double check with stratospheric wind data. Here we use MERRA data (see Appendix fig. 37).

It is essential to identify the major SSW by the mean zonal wind in the radar data. Without a proper removal of the strong amplitudes of the atmospheric tides, results can be biased.

In figure 19 the zonal wind ± 90 days around the major SSW onset in 2009, the 23.01.2009, is shown. Here the tides aren't removed and so there are strong amplitudes in positive as well as in negative direction. Around the day +70 the final warming can be recognized, which marks the transition from winter to summer circulation. Around the days -60, -40 and the central day stronger negative amplitudes occur. From this figure it is not clear, whether the negative wind occurred due to SSWs or tides. In figure 20 the mean zonal wind is shown. The tides are removed and so the variability is decreased, apart from the strong negative wind around the central day and the strong positive wind a few days after the central day. Concluding, the strong negative wind around the central day is identified as the major SSW event. The strong increased positive wind after a SSW event is observed in other years as well, e.g. in 2004 and 2006.

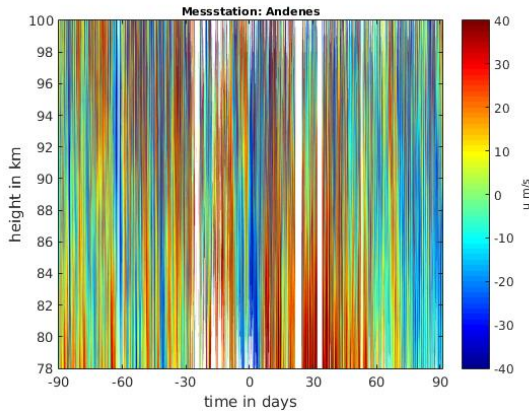


Figure 19: Zonal wind with tides for the period ± 90 days centered around 23.01.2009.

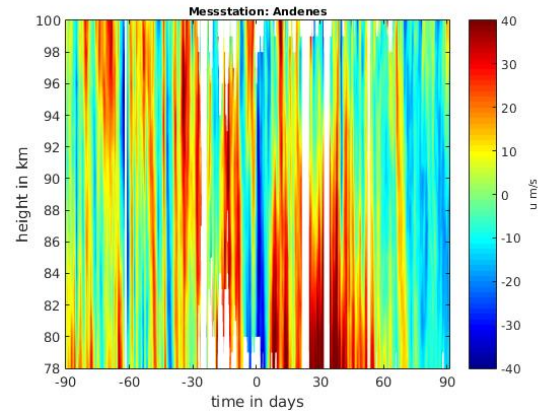


Figure 20: Mean zonal wind for the period ± 90 days centered around 23.01.2009.

4.2 Gravity wave activity and momentum flux around SSWs

4.2.1 Gravity wave activity

To examine a possible relation between gravity wave activity and strength of the momentum flux during a SSW, the gravity wave activity within a period of ± 10 days around the onset day is analyzed. Moreover it shall be considered how the gravity wave activity varies under the influence of a major warming event.

Histograms of the residual radial velocity for every height bin and every day are set up. The variances of the residual radial velocities are a proxy of the intensity of the gravity wave activity. In figure 21 histograms of the residual radial velocities are shown, for three height regions (region 1: 84-85 km, region 2: 89-90 km, region 3: 93-94 km) at the onset day 23.01.2009. The standard deviation, which is the square root of the variance, is for the first region 13,3001 m/s, for the second region 23,6852 m/s and for the third region 11,5921 m/s. So first the gravity wave activity increases from 84-85 km to 89-90 km but then decreases from 89-90 km to 93-94 km again. This could be explained by gravity waves, which break around the heights of 89-90 km. Since after the breaking the standard deviation is not zero, there is still some gravity wave activity left. So either the broken waves have not transferred all of their momentum to the background wind and so they

can propagate further but with smaller amplitudes, there are secondary generated waves or not all gravity waves break at that altitude.

In the figures 22, 23, 24, 25, 26, 27 and 28 contour plots of the variances of the residual radial velocities, from 78-100 km for the period ± 10 days around the SSW onset, are shown. Especially in the years 2004, 2006 and 2010 (fig. 22, 23 and 24) the gravity wave activity is stronger before the SSW onset than after the SSW event. Furthermore it should be noted, that the magnitude of the variance differs significantly. The variance reaches, during the SSW event in 2004, maximum values of $70 \text{ m}^2/\text{s}^2$, in 2006 maximum values of $600 \text{ m}^2/\text{s}^2$ and in 2010 even maximum values of $1100 \text{ m}^2/\text{s}^2$. During the SSW in 2006 and 2010 the state of the increased variance before the SSW onset lasts at least over 7 days and reaches from 85 to 92 km. In the year 2004 the state of the increased variance before the SSW onset is not that consistent as in the years 2006 and 2010, but there are still regions of larger variance before the SSW event, e.g. from day -10 to day -8 or from day -4 to day -1, at regions from 85 to 92 km.

Unlike the variance distributions during the SSW periods in 2004, 2006 and 2010 the variance of the residual radial velocity is not larger before the SSW onset in the year 2009 (fig. 25). Around day -8 day from 87 to 90 km the variance is increased to values of $120 - 140 \text{ m}^2/\text{s}^2$ and from day -7 to day +3 the variance does not exceed values of $70 \text{ m}^2/\text{s}^2$. At the +5th and +10th day the variance reaches maximum values of approximately $220 \text{ m}^2/\text{s}^2$.

In figure 26 the variance of the residual radial velocity is shown, also for the period ± 10 days around the SSW onset in 2009. Those measurements were taken in Juliusruh instead of Andenes. Here the variance distribution is similar to these ones from 2004, 2006 and 2010. There is a continuous state of increased variance from day -10 to the onset day 0 in regions between 84 to 92 km with maximum values of $700 \text{ m}^2/\text{s}^2$. Around day +5/6 the variance is also increased, but doesn't reach the maximum values.

In figure 27 the variance distribution for the period ± 10 days around the SSW onset in 2013 is shown. From day -9 to day +8 the variance is continuously enhanced with maximum values of $1100 \text{ m}^2/\text{s}^2$. The period of increased variances reaches from 83-84 km up to 93 km. Except for the period from day -9 to day -6, where the state of enhanced variance reaches from 86 km up to 93 km. The

variance distribution in figure 27, which was measured in Andenes, looks quite special. Therefore the variance distribution for the same period but measured in Juliusruh is considered in figure 28 for comparison. In figure 28 there is no such a long period of continuously enhanced variances as it is determined for Andenes in 2013 (fig. 27). Instead there are regions of increased variances around day -4/-3 from 83 km up to 92 km and from day +4 to day +7 from 85 km up to 90 km, with maximum values of $550 \text{ m}^2/\text{s}^2$. So the pattern of increased gravity wave activity before the SSW onset day is not observed, as it is the case during the events in 2004, 2006 and 2010.

There is the assumption, that the gravity wave activity during a SSW depends from the position and strength of the polar vortex. This assumption is analyzed in the chapter 'Discussion'.

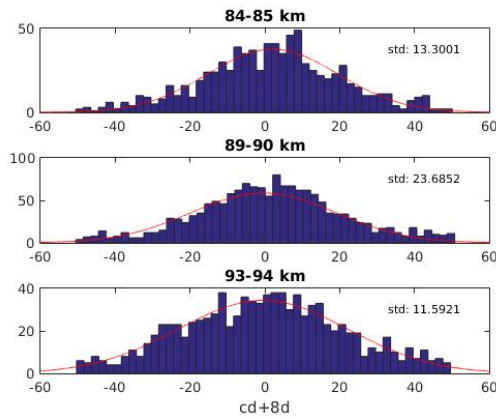


Figure 21: Histograms of the residuals of radial velocities for three different height regions.

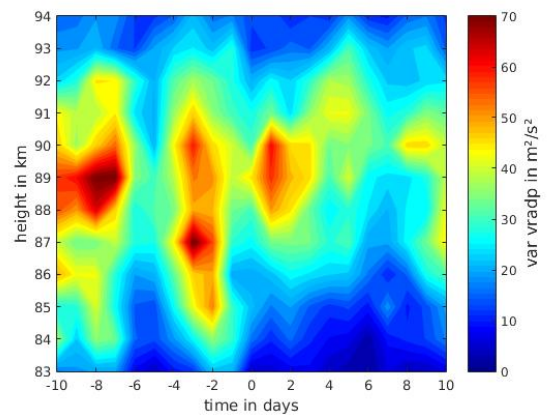


Figure 22: Variance distribution for the period ± 10 days centered around 6.01.2004 (measured in Andenes).

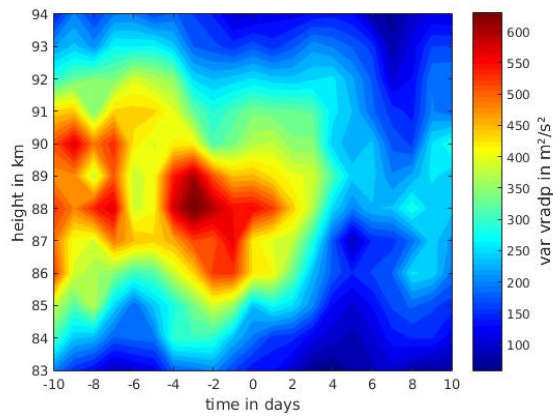


Figure 23: Variance distribution for the period ± 10 days centered around the 20.01.2006 (measured in Andenes).

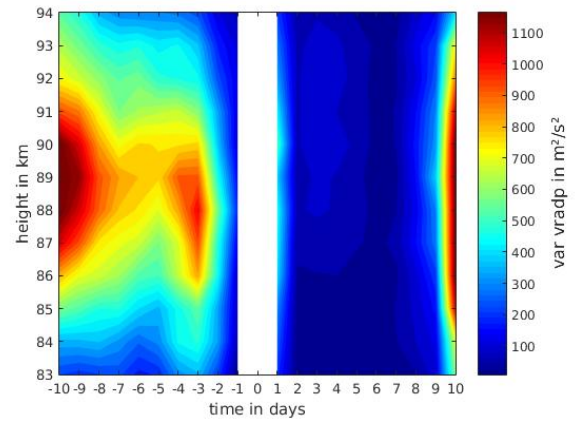


Figure 24: Variance distribution for the period ± 10 days centered around the 28.01.2010 (measured in Andenes).

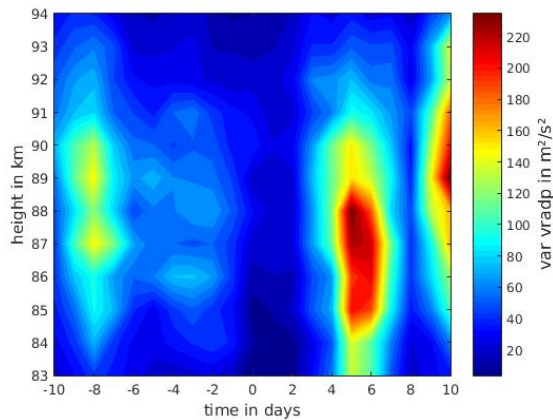


Figure 25: Variance distribution for the period ± 10 days centered around the 23.01.2009 (measured in Andenes).

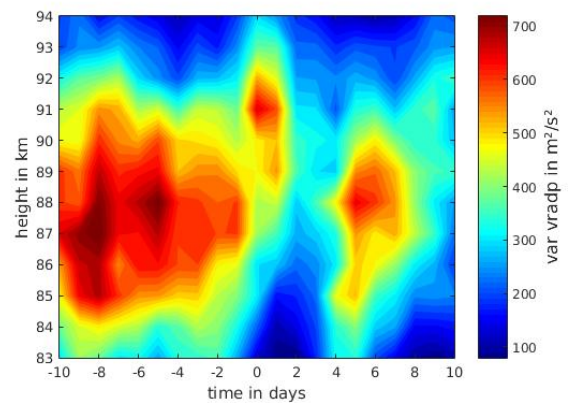


Figure 26: Variance distribution for the period ± 10 days centered around the 23.01.2009 (measured in Juliusruh).

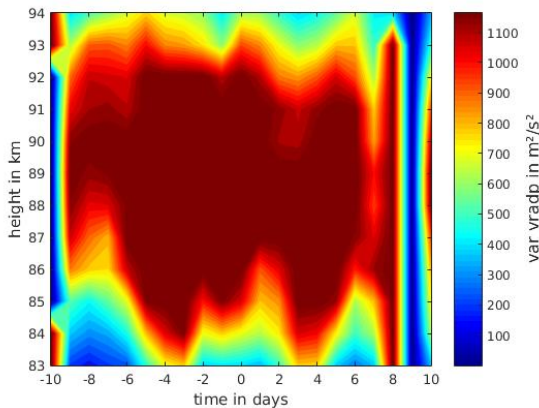


Figure 27: Variance distribution for the period ± 10 days centered around the 07.01.2013 (measured in Andenes).

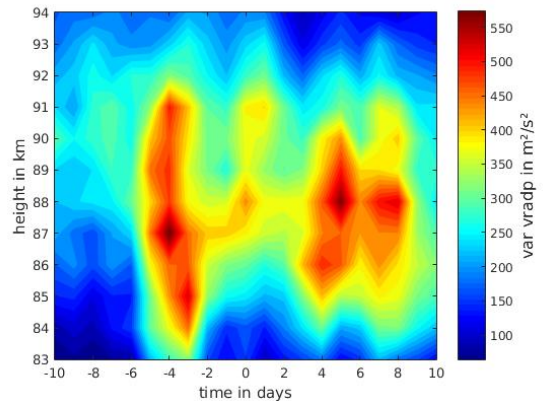


Figure 28: Variance distribution for the period ± 10 days centered around the 07.01.2013 (measured in Juliusruh).

4.2.2 Momentum flux

In the following paragraph we perform a more sophisticated analysis by investigating the momentum flux for similar SSW events as before. The momentum flux for the periods ± 30 days around the SSW onset in 2004, 2006, 2009, 2010 and 2013 is calculated by applying the Hocking method described in section 3.5. In the figures 29, 30, 31, 32 and 33 the mean zonal wind and the momentum flux for several major warming events from 78 km up to 100 km are shown. The data for the calculation of the wind and the momentum flux are recorded by the meteor radar in Andenes.

Figure 29 shows in the upper panel the mean zonal wind and in the lower panel the gravity wave momentum flux for the period ± 30 days around the SSW onset in 2004 (06.01.2004). The central day is the SSW onset. The prevailing wind during the period is mainly positive, as it is typical for winter (cf. *Andrews et al. (1989)*). Around day -25 and day -14 the wind reaches larger velocities of approximately 15 m/s and around day -5 at heights from 90 up to 100 km the wind reaches values of 25 m/s . The wind reversal lasts from the central day until 5 days after. During this short period the wind reaches values of $-15 m/s$. After that the mean zonal

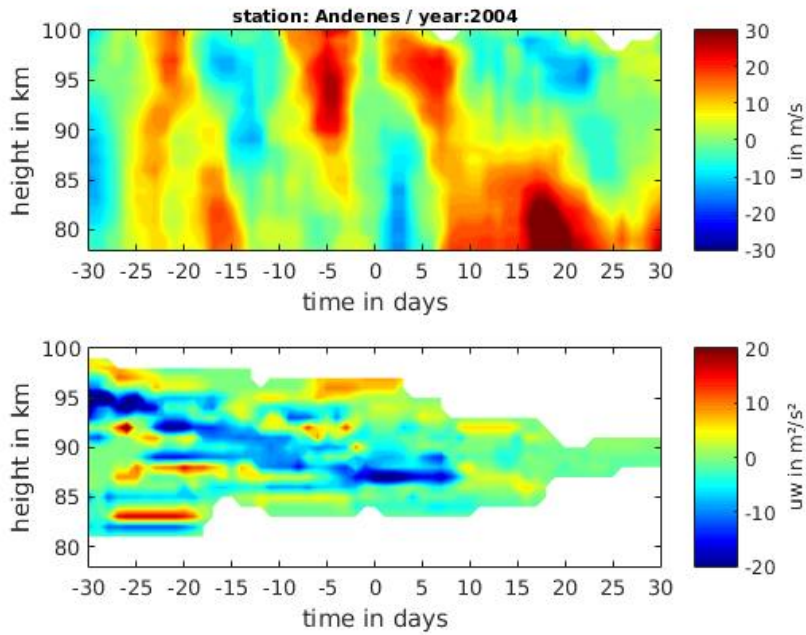


Figure 29: Mean zonal wind (upper panel) and gravity wave momentum flux (lower panel) for the period ± 30 days centered around 06.01.2004 (SSW onset)

wind reverses positive again with even larger speeds of up to 40 m/s than before the SSW.

The momentum flux for the period around the SSW in 2004 could not be calculated for all days and heights. Since there were too less meteors observed, it could not determined a reliable momentum flux in the periods from day -30 to day +15 in heights from 78 to 83 km and from day +15 to day +30 from 78 km up to 86 km. Furthermore, there is no momentum flux determined from 98 km up to 100 km over the entire period. From day +5 on to day +30 there is also no reliable momentum flux from approximately 93 km up to 100 km. The momentum flux which was calculated has moderate positive as well as negative values of up to $\pm 15 \text{ m/s}$. Whereas the negative momentum flux dominates during the period from day -30 to day +5. After that the momentum flux takes smaller values of $\pm 5 \text{ m/s}$ from day +5 on. Whereby the positive velocities dominate.

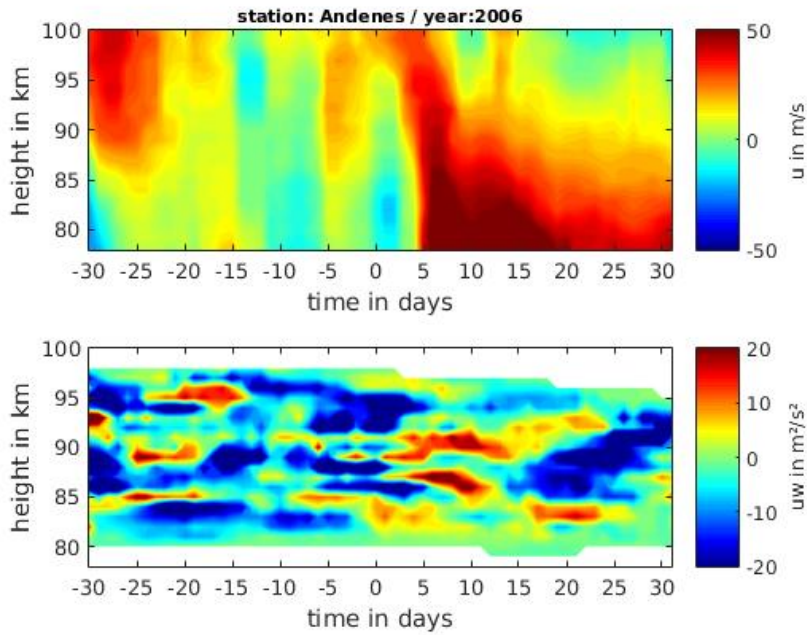


Figure 30: Mean zonal wind (upper panel) and gravity wave momentum flux (lower panel) for the period ± 30 days centered around 20.01.2006 (SSW onset)

In figure 30 the mean zonal wind and the gravity wave momentum flux for the period ± 30 days around the SSW onset in 2006 (20.01.2006) is shown. The SSW onset in 2006 cannot clearly be identified by the mesospheric mean zonal wind in the upper panel, since there is also a wind reversal around day -8. Eventually the stratospheric MERRA data shows, that there is only a wind reversal at 10 hPa at the 20.01.2006. So this date is chosen to be the SSW onset. Except for the period around day -8 the mean zonal wind before the SSW event is mainly moderate eastward. Around day -30 to day -20 at heights from 85 km up to 100 km there is a very strong eastward wind with velocities of approximately $30 - 40 \text{ m/s}$. At the central day the wind changes its direction and reaches values of -15 m/s . After the wind reversal the mean zonal wind is positive again with very strong amplitudes of 50 m/s . These strong amplitudes occur from 78 km up to 100 km from day +5 to day +9. From the +10th day on there are still strong positive prevailing winds at the height regions from 78 to 95 km.

In the lower panel of figure 30 the gravity wave momentum flux is shown. The

momentum flux is mainly negative. However there are patches indicating also positive momentum flux, e.g. in the period from day -25 to day -15 at 90 km and 95 km and on day -5 at 85 km. Moreover positive momentum flux is observed over the period from the central day to day +20 from 78 to 93 km.

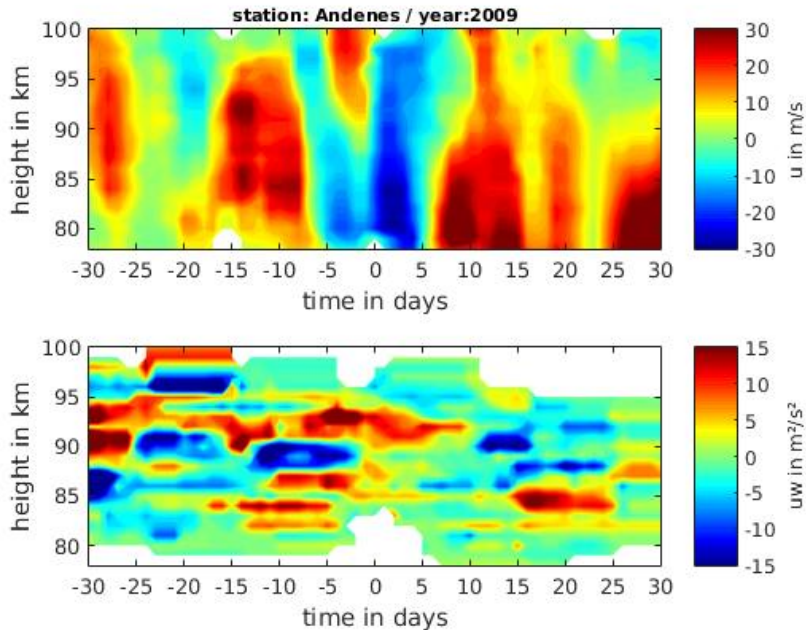


Figure 31: Mean zonal wind (upper panel) and gravity wave momentum flux (lower panel) for the period ± 30 days centered around 23.01.2009 (SSW onset)

In figure 31 the mean zonal wind and the gravity wave momentum flux for the major warming in 2009 is shown. From day -30 to day -5 positive wind dominates. Whereas around day -30 and from day -20 to day -6 the wind has stronger amplitudes of approximately 20 m/s . From day -5 the wind changes direction and turns negative. Around the central day, the 23.01.2009, the negative wind is very strong with velocities of -20 to -30 m/s over all heights. The negative wind stays until day +5. Then the wind is positive again, with even stronger amplitudes of 30 m/s than before the major warming. The momentum flux for the period ± 30 day around the SSW onset in 2009 distinguishes strongly from the momentum flux for the period in 2006. It is apparent that during the period from day -30 to the

central day the momentum flux in positive as well as in negative direction, with values of up to $\pm 15 \text{ m}^2/\text{s}^2$ and is larger than after the SSW. Furthermore one should note the continuously positive momentum flux from day -30 to day +10 at heights of approximately 92 to 94 km. Apart of the strong momentum flux in the period from day +15 to day +25 at 85 km the momentum flux tends to be small with values around $0 \text{ m}^2/\text{s}^2$ after day +5.

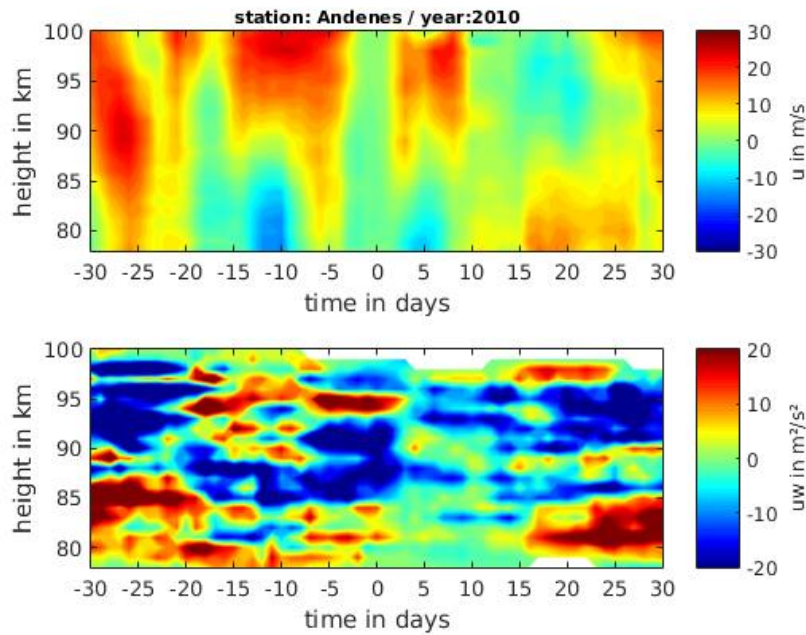


Figure 32: Mean zonal wind (upper panel) and gravity wave momentum flux (lower panel) for the period ± 30 days centered around 28.01.2010 (SSW onset)

In figure 32 the mean zonal wind and the gravity wave momentum flux for the major warming in 2010 is shown. From day -30 to day -20 the wind is positive with values up to 25 m/s at all heights from 78 to 100 km. From day -20 the wind changes its direction and shows velocities of approximately -10 m/s . Around day -12 the negative wind reaches its maximum of -15 m/s . On day -5 the wind turns to positive directions again, but just for a couple of days. During the period from day -15 to day -4 the wind is negative at heights from 78 km to 90 km. Above the prevailing wind is positive with values up to 25 m/s . From day -5 to day +3 the

wind has weak with velocities varying between 1 m/s and -3 m/s at all heights. The central day, the 28.01.2010, is the SSW onset. Since it could not certainly determined by the mesospheric wind data, the stratospheric MERRA data was also considered for the identification of the SSW onset. Unlike the years before, the mean zonal wind in 2010 does not turn back shortly after the SSW event to positive directions with even stronger amplitudes than before. The wind remains negative till day +10 instead, apart of a couple of days around day +5 in heights from 88 to 100 km. Eventually from the +10th day on the wind is positive again with moderate velocities of 10 to 15 m/s .

The momentum flux shows some similarities to the momentum flux for the periods in 2004, 2006 and 2009. As it is observed in 2004 and 2009 the momentum flux is weaker during the two weeks after the central day. Moreover a stronger positive momentum flux arises from day +15 on at heights from 78 to 85 km. This is also observed in 2006 and 2009. For the momentum flux in 2004 it is not possible to draw conclusion regarding this observation, since there were too less meteors around this period. So no reliable momentum flux could be calculated. Before the central day the momentum flux in 2010 is positive as well as negative, with maximum values of $\pm 30\text{ m}^2/\text{s}^2$. Whereas the momentum flux from day -30 to the central day from 78 km up to 85 km is mainly positive and from 85 km to 90 km negative. Above 90 km during the period from day -30 to day -15 the momentum flux is negative and from day -15 to the central day it is positive. As observed in the years 2006, 2009 and 2010 the momentum flux is in the period of approximately ten days after the central day weaker than before the SSW event. Also there is a strong positive momentum flux with maximum values of $20\text{ m}^2/\text{s}^2$ observed from day 7 on in heights of 85-90 km. From day -30 to the central day strong negative momentum flux dominates with amplitudes of $-20\text{ m}^2/\text{s}^2$.

In figure 33 the mean zonal wind and the gravity wave momentum flux for the period ± 30 days from the SSW onset day in 2013 is shown. The SSW onset is determined as the 7.01.2013. Apart from the wind reversal around the central day, a positive mean zonal wind dominates. From day -30 to day -25 the wind has stronger amplitudes between $15 - 20\text{ m/s}$ at all heights. During the period from the central day to day +5 the wind changes direction and becomes negative

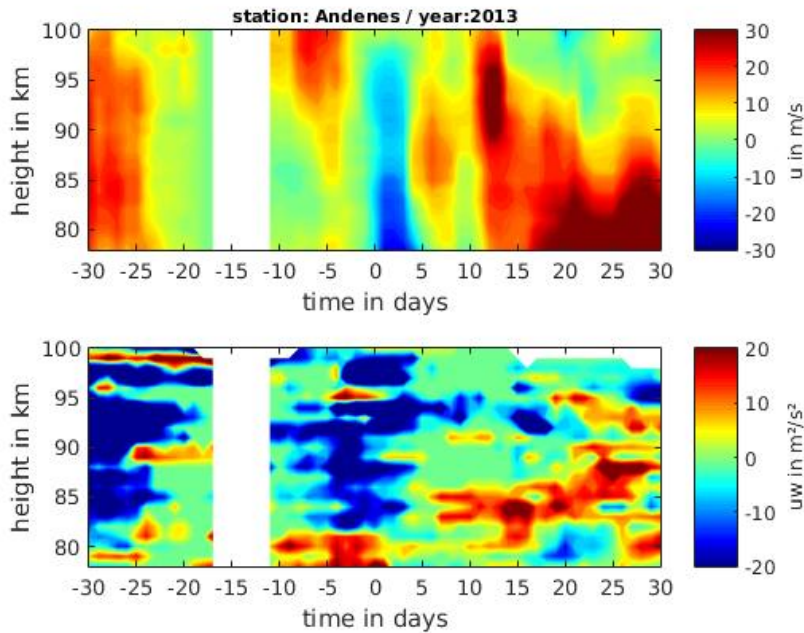


Figure 33: Mean zonal wind (upper panel) and gravity wave momentum flux (lower panel) for the period ± 30 days centered around 07.01.2013 (SSW onset)

with amplitudes of -25 m/s . After that the zonal mean wind turns back again. Whereas the wind reaches values of up to 30 m/s from day 11 on.

In figure 34 the composites of the mean zonal wind and the gravity wave momentum flux for the major events in 2004, 2006, 2009, 2010 and 2013 are shown. In general the mean zonal wind is positive in winter time. This is also observed during the period ± 30 days from the SSW onset, apart from the wind reversal around the central day. Before the SSW onset the dominating wind is moderate positive ($0 - 15 \text{ m/s}$). Whereas from day -30 to day -25 and around day -5 the amplitudes are stronger with approximately 20 m/s at heights of 85 up to 100 km. Around the central day the wind changes direction and reaches values of up to -15 m/s . From day +5 the wind is positive again with amplitudes of 20 m/s and maximum values of 30 m/s from day +20 to day +30. The momentum flux from day -30 to the central day is mainly negative with maximum values of $-10 \text{ m}^2/\text{s}^2$. However there is also positive momentum flux observed

during this period, at the height region of 78 to 80 km. Around the central day the momentum flux weakens to around $0 \text{ m}^2/\text{s}^2$. This state lasts approximately for 10 days. From day +10 on the momentum flux becomes stronger in positive as well as in negative direction. At heights of 78 up to 85 km positive and from 85 up to 100 km negative momentum flux is observed.

Finally one should note, that the wind does not change strongly with height, rather with the time. Instead the momentum flux strongly depends on the height. For example, at day -15 the momentum flux is positive at 85 km and negative from 86 to 91 km and turns to positive values again from 92 up to 95 km.

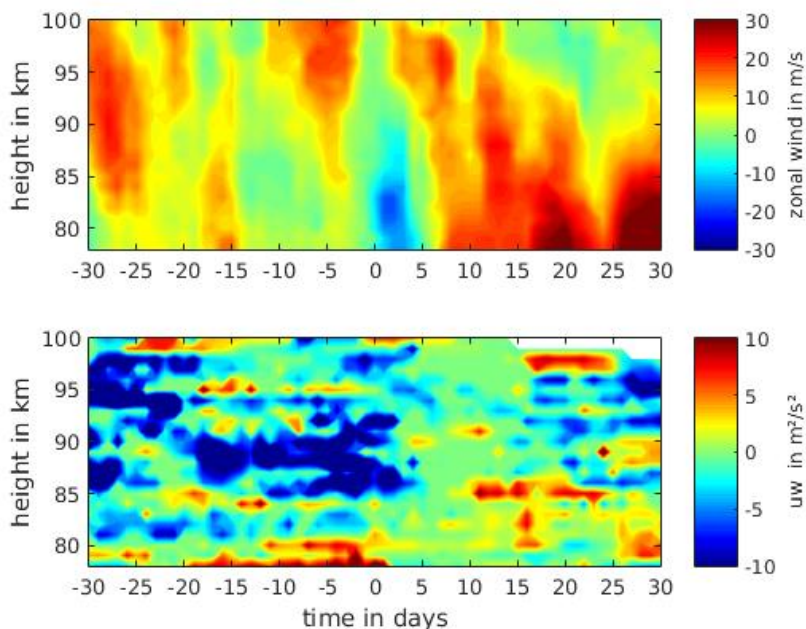


Figure 34: Composites of mean zonal wind (upper panel) and gravity wave momentum flux (lower panel) for the period ± 30 days centered around the SSW onset

4.3 Annual variation

In the following composites of annual variations of the zonal mean wind and the gravity wave momentum flux for years with and without a major warming are

described between 2004 and 2014.

In figure 35 in the upper panel the composite of the annual mean zonal wind variation and in the lower panel the annual momentum flux variation is shown including the years 2005, 2007, 2008, 2011, 2012 and 2014. In those years no major warming event appeared. The zonal wind shows a typical annual variation (e.g. *Andrews et al.* (1989)). In winter time, that means during periods from the beginning to day 90 and from day 270 to day 365, the zonal mean wind is positive over all heights from 78 up to 100 km. During these periods the wind velocities are approximately 10 m/s . With the end of the winter the wind changes its direction and becomes negative. From day 90 to day 150 the wind velocities are $-10 m/s$ at all heights. Then from day 150 to day 240 the wind reaches even values of up to $-35 m/s$. However the negative zonal wind during this period does not reach over all heights, but from 78 km to approximately 90 km. Whereas the upper limit of the negative wind decreases from 92 to 89 km during the period from day 150 to day 240. Above the upper limit, the wind reverses and reaches very strong positive amplitudes of 30 m/s .

There are two interesting observations regarding to the gravity wave momentum flux one should note. From 78 to 90 km the momentum flux is mainly positive with moderate positive values during the first 90 days and maximum values of up to 15 m^2/s^2 during summer time. Between 90 km and 100 km the momentum flux is kind of anticorrelated to the zonal wind. Thus the momentum flux during the period from day 0 to day 90 is mainly negative, turns positive from day 90 to day 220 and becomes negative again from day 230 until the end of the year.

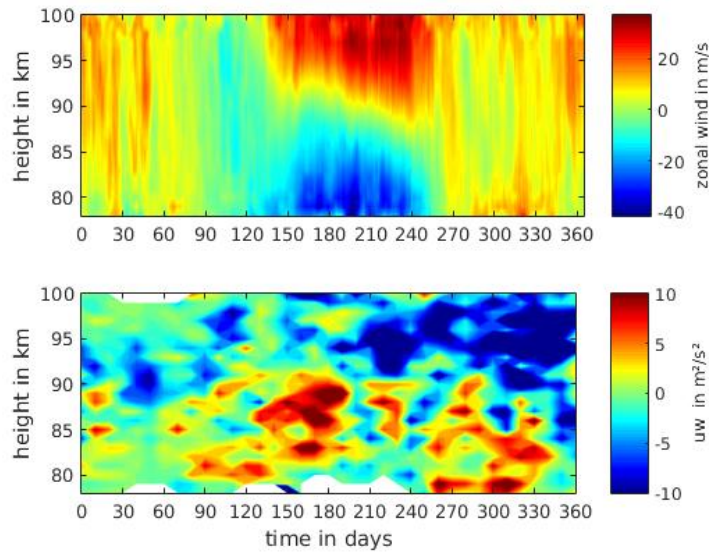


Figure 35: Composites of mean zonal wind (upper panel) and gravity wave momentum flux (lower panel) variations in years without a major warming event

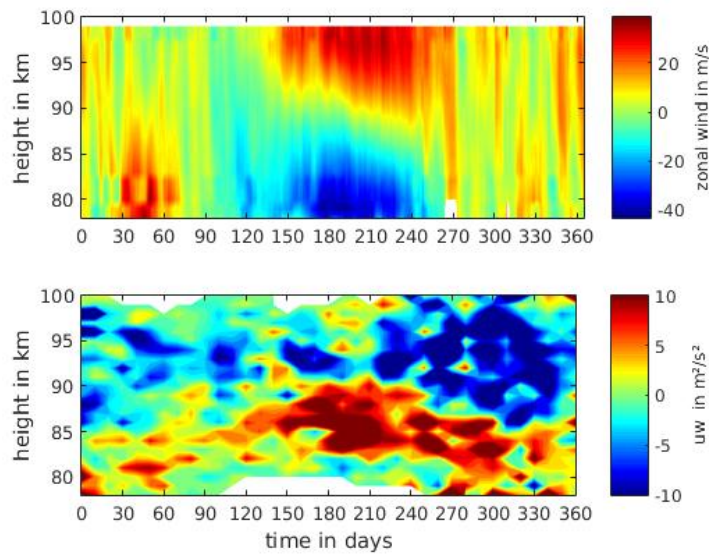


Figure 36: Composites of mean zonal wind (upper panel) and gravity wave momentum flux (lower panel) variations in years with a major warming event

In figure 36 the composites of the annual mean zonal wind variation and the annual gravity wave momentum flux variation including the years 2004, 2009, 2010 and 2013 are shown. In those years a major SSW occurred. The mean zonal wind shows also the typical variation as it was observed in figure 35. The prevailing wind is in winter time positive and in summer time negative. However there are differences to the zonal mean wind shown in figure 35. For example, from day 30 to day 60 the positive wind reaches large velocities up to 30 m/s at heights from 78 to 85 km and is stronger than it is observed in the composite of the years without a major warming event. Above 85 km the positive wind decreases to velocities between $\pm 9 m/s$ and becomes weaker than the wind in figure 35 for the same period and height region. Another difference between the composites of the wind variation for years with and without major warmings is the stronger negative wind around day 120. There it reaches values of -25 m/s . Furthermore the negative wind from day 180 to day 210 from 78 to 80 km is stronger than in figure 35. From day 270 on the wind turns positive again. Whereas the wind around day 270 reaches values of almost 20 m/s and is stronger than the wind around those days in the years without a major warming. After the 270th day the prevailing positive wind is weaker than the wind during this period in years without a major warming.

The momentum flux shows similarities as well as differences to the momentum flux in figure 35. They have in common that from 78 to 85 km the positive momentum flux dominates. Furthermore the momentum flux in figure 36 shows also the anticorrelation to the mean zonal wind from 85 up to 100 km. There are differences in the strength of the momentum flux in positive as well as in negative direction. So the positive momentum flux during the period from day 0 to day 90 in heights from 78 km to 85 km is stronger than in figure 35. Furthermore a stronger negative momentum flux from 85 km to 100 km for the same period is observed. Moreover, the momentum flux during summertime is at heights from 78 km to 90 km continuously positive and also continuously stronger than in the composite of the years without a major warming.

5 Discussion

5.1 Gravity wave activity and momentum flux around SSWs

5.1.1 Gravity wave activity during SSW periods

As described by *Wang and Alexander* (2009) the gravity wave activity in the lower mesosphere decreases during SSWs. Due to the wind reversal in the stratosphere, gravity waves are filtered out and consequently the gravity wave activity is reduced in the mesosphere.

This observation coincides partly with the calculated gravity wave activities presented in this thesis (fig. 22-28). In the years 2004, 2006 and 2010 an enhanced gravity wave activity is observed before the SSW onset. Note, that the enhancement is the strongest before the SSW 2010 and the weakest before the SSW 2004. Moreover the gravity wave activity weakens during the SSW in those years. In 2009 the gravity wave activity is still enhanced before the SSW, but the strongest activity is observed approximately 5 days after the SSW onset. The gravity wave activity during the period ± 10 days from the SSW onset in 2013 shows a very special distribution. Here the activity is strongly enhanced from day -9 to day +8 over all ranges. The activity variations for the SSWs 2009 and 2013 are quite different compared to the other years. Hence it was also considered the gravity wave activity in Juliusruh for the SSW 2009 and the SSW 2013. All the described observations before were with regards to the meteor radar in Andenes. The gravity wave activity in Juliusruh shows a stronger enhanced activity before the SSW 2009. But around day +5 exists still the enhancement of gravity wave activity, which is also observed in Andenes. During the SSW 2013 it occurs a weaker activity in Juliusruh than in Andenes. Here an enhancement before the SSW onset and short weakening during the SSW event is observed. Approximately 4 days after the SSW 2013 onset the gravity wave activity increases.

One possible reason for the differences in the gravity wave activity variations could be the position related to the polar vortex. Many studies have reported a dependence of the gravity wave activity on the position to the polar vortex, e.g. *Wang and Alexander* (2009) or *Whiteway et al.* (1997). According to those studies, a high gravity wave activity is expected at the edge of the polar vortex. Within the

vortex core and outside of the vortex the activity is weaker. In fact, the polar vortex edge is located further away from Andenes before the SSW 2009 than after (see Appendix fig. 38-42). It is located even quite close to Andenes approximately 6 days after the SSW onset 2009. This would explain the gravity wave activity enhancement at this time. In addition, Juliusruh is closer to the polar vortex edge before the SSW onset 2009. Hence the observed gravity wave activity is stronger before the SSW onset than in Andenes at this time.

Moreover, the polar vortex edge is located very close to Andenes from the 01.01.2013 to the 12.01.2013. That fact coincides with the strong gravity wave activity lasting over nearly the same period. Considering that, Juliusruh is also close located to the vortex edge, but the gravity wave activity is not that strong than in Andenes. A possible explanation could be, that Juliusruh is mainly located outside of the polar vortex during the considered period of ± 10 days from the SSW onset 2013.

The idea was, to compare the variation of the gravity wave activity and the momentum flux. One would expect, that an enhanced gravity wave activity results in an enhanced momentum flux. As a matter of fact, it could not be determined any certain relation for all events. Only the SSW 2010 is an exception, since the variation of the gravity wave activity and the strength of the momentum flux correspond with each other. However, for the other events there is no such a relation identified. That can be explained perhaps by the fact, that gravity wave activity does not mean instantaneous wave breaking. Indeed, the momentum flux is only transferred when the waves break. In further analysis regarding the relation between momentum flux and gravity wave activity, extended height ranges should be considered.

Note, that the determination of the gravity wave activity is done by the variance of the residual radial velocity. So the variance consists of the variances of the zonal, meridional and vertical components. That fact complicates the comparison with the zonal gravity wave momentum flux. However, it is not recommended to determine the gravity wave activity by the residual of the zonal wind component. The inaccuracies of the calculated zonal wind are higher than the inaccuracies of the radial velocity, since the radial velocity is directly observed by the radar.

5.1.2 Gravity wave momentum flux during SSW periods

In *Körnich and Becker* (2010) it was shown by model data of KMCM that a major SSW event can change the filtering conditions for vertically propagating waves. Hence the released momentum flux of breaking gravity waves can change the strength or even direction of the momentum flux. According to *Holton and Alexander* (2000), the momentum flux induces a force that accelerates or decelerates the zonal background wind. That force is called the gravity wave drag.

Usually the mean zonal wind is positive in winter time. Gravity waves with negative or strong positive phase velocities are able to propagate upwards to the mesosphere. When those waves break, they transfer their momentum flux to the background wind. Due to dominating gravity waves with negative phase velocities, the momentum flux is negative in winter. The negative wave drag causes a deceleration of the zonal background wind.

In case of a major warming the mean zonal wind changes direction and turns positive for a couple of days. During the wind reversal the filter conditions change and hence gravity waves with positive phase velocities can propagate up to the mesosphere. Whereas gravity waves with moderate negative phase velocities are filtered out. As a consequence the dominating positive momentum flux reduces the negative momentum flux or even turns it from negative to positive during this period. This causes an acceleration of the mean zonal wind, due to the positive wave drag.

In the present thesis the mean zonal wind and the gravity wave momentum flux for the period ± 30 days from the SSW onset at heights from 78 km to 100 km are considered. The observed mean zonal wind is positive according to typical winter conditions. During the major warming event the mean zonal wind becomes negative for a couple of days. After the SSW event the mean zonal wind turns positive again. Apart from the year 2010, the positive post SSW wind is enhanced. That enhancement is also described in other studies, e.g. *Hoffmann et al.* (2007).

The observations regarding the momentum flux in the present thesis correspond

to the results of *Körnich and Becker* (2010). In figure 34 the momentum flux before the SSW onset is mainly negative. Whereas after the SSW event positive momentum flux dominates, especially at heights up to 85 km. Furthermore one should note, that during the approximately 10 days after the SSW event, the momentum flux in figure 34 is weaker and shows mainly values between $0 \text{ m}^2/\text{s}^2$ and $+3 \text{ m}^2/\text{s}^2$. The described accordance refers to the composite of the momentum flux. Considering the separate SSW events, there also exist exceptions, e.g. in 2006 (fig. 30). There is no weakening of the momentum flux observed after the SSW. However in 2006 is a strong positive momentum flux observed after the SSW. That would explain, that the enhancement of the mean zonal wind after the SSW in 2006 is the largest of the observed major warmings periods.

The strongest weakening occurs after the SSW event in 2010. It is apparent, that the wind reversal in 2010 is the weakest of the considered major warmings. Gravity waves with eastward as well as westward phase velocities are able to reach the mesosphere. Thus the momentum flux is compensated with values approaching $0 \text{ m}^2/\text{s}^2$. Furthermore, no enhancement of the mean zonal wind occurs after the SSW 2010.

The post SSW positive momentum flux in the composite in figure 34 lasts over 30 days. This is a quite long response for an event, which lasts only a couple of days. Indeed, one should take into account that in this thesis wind and momentum flux at ranges from 78 km to 100 km are considered. A possible vertical coupling of stratospheric dynamics cannot be identified by only mesospheric data. Stratospheric mean zonal wind data provided by MERRA (see Appendix fig. 37) shows, that the mean zonal wind during the most major warmings stays negative at least for 10 days from the SSW onset. That could be a possible explanation for the long period of positive momentum flux after the SSW. Moreover it explains the strong enhanced positive mean zonal wind in the mesosphere after the SSW event. As a result of stratospheric filtering of gravity waves with negative phase velocities, the gravity wave drag in the mesosphere is positive and accelerate the zonal background wind. The longer the period of negative mean zonal wind in the stratosphere lasts, the stronger is the influence of the positive wave drag on the zonal background wind in the mesosphere. As a matter of fact, the strongest enhancement of the positive mean zonal wind in the mesosphere after the SSW 2006

coincides with the longest period of negative mean zonal wind in the stratosphere. The period of negative mean zonal wind in the stratosphere during the SSW 2010 is the shortest of the considered major warming events. In fact, no enhancement of the positive mean zonal wind in the mesosphere after the SSW 2010 is observed. The relation between the duration of the period of negative mean zonal wind in the stratosphere during the SSW and the strength of the enhancement of positive mean zonal wind in the mesosphere is also consistent for the other considered major warming events.

The strong positive mean zonal wind after the SSW in the mesosphere may prevent further propagation of gravity waves with positive phase velocities. This results in a negative momentum flux from 85 km upwards (fig. 34), due to dominating gravity waves with negative phase velocities. As a consequence it is induced a negative wave drag above 85 km, which decelerate the mean zonal wind at heights above 85 km.

Bear in mind, that the here considered stratospheric mean zonal wind belongs only to the 10 hPa level. For further analysis of the coupling of stratospheric and mesospheric dynamics it is recommended to involve the mean zonal wind and momentum flux for the entire stratosphere.

Another interesting point is, that the momentum flux varies strongly with the height and less with time. In contrast to the mean zonal wind, which does not change strongly with height rather with time. At this point it should be mentioned that the momentum flux was averaged over 10 days, whereas the mean zonal wind was averaged over 6 days. This would explain that the momentum flux changes less with time than the mean zonal wind. But it is no explanation for the strong variation of the momentum flux with height. This observation could be explained by waves, which become instable at mesospheric heights due to their large amplitudes. According to *Lindzen* (1981) those waves generate turbulences to prevent further amplitude growth. Moreover it could be possible, that those turbulences generate new waves. This wave breaking and generation of wave induced turbulenc could be a possible explanation for the observed momentum flux variation with height.

The determination of the gravity wave momentum flux stated by *Hocking* (2005) is an established method (e.g. *Antonita et al.* (2008), *Placke et al.* (2011), *de Wit et al.* (2014)). The starting point of this method is the minimization of the difference between the squared residual radial velocity and the squared model residual radial velocity (see chapter 3.5). A possible error source could be the residual radial velocity. It is the difference between the measured radial velocity and the fitted radial velocity. The fitted radial velocity consists of the mean zonal wind including planetary waves with long periods ($T \geq 10 d$) and the terdiurnal, semidiurnal and diurnal solar tides. Planetary waves with shorter periods are not involved. During winter that should not have a strong impact since the 4-day and 5-day wave reach quite large amplitudes primary during seasonal transitions (*Fedulina et al.* (2004)). But the missing of the semidiurnal tide in the fit may have an impact on the residual radial velocity, as it was observed to peak during SSWs and is able to reach amplitudes of 40 m/s (*Chau et al.* (2015)).

It should be mentioned, that the momentum flux was calculated for the same period (01.12.2012 - 28.02.2013) and minimum amount of meteors (30) as it is represented in *de Wit et al.* (2014) for verification (see Appendix fig.49). A comparison shows, that the momentum flux variations are quite similar, but have opposite sign. Following control calculations could not identify a mistake. Moreover, the calculated annual variation of the momentum flux shows accordance to the results in *Placke et al.* (2011).

For the sake of completeness, the mean meridional wind was also considered. Since it could not be established any relation between mean meridional wind and gravity wave momentum flux, the mean meridional wind was not further discussed. The composite of the mean meridional wind of the considered SSW periods is listed in the Appendix (fig. 48).

In addition, the terdiurnal, semidiurnal and diurnal tides were plotted separately for the period ± 30 days centered around the SSW onset. This is done for all of the major warmings, considered in the recent thesis (see Appendix fig. 43-47). The tides vary strongly from year to year, whereby the semidiurnal tide has always the largest amplitudes. It could not be determined a response of the tides to the major warming events.

5.2 Annual variation of the gravity wave momentum flux

Under normal conditions the mean zonal wind is positive in winter and negative in summer up to the lower mesosphere. In the upper mesosphere, the positive mean zonal wind in winter decreases and in summer it even changes its the direction - from negative to positive.

That annual wind variation is also observed in the composites of the mean zonal wind for years without a major warming event (fig. 35) and for years with a major warming event (fig. 36). However, both composites differ in some points.

The composite of years with a major warming shows a weaker positive mean zonal wind during the first 30 days than the composite of years without a major warming. This is probably caused by the wind reversal, which accompanies the major warming event. From day 30 to day 60 at heights up to 88 km, the positive mean zonal wind is strongly enhanced in the composite of years with a major warming. The mean zonal wind reaches even velocities, which are as twice as high than in the composite of years without a major warming during the same period. That strong positive mean zonal wind is probably related to the often observed post SSW enhancement of the positive mean zonal wind. Above 88 km in the period from day 30 to day 60 the mean zonal wind velocity tends to 0 m/s and is weaker than in the composite of years without a major warming.

Further occurs a stronger negative mean zonal wind around day 120 in the composite of years with a major warming than in the composite of years without a major warming at this time up to 87 km. Above 87 km the negative velocity in the composite of years with a major warming decreases and tends to 0 m/s and becomes weaker than in the composite of years without major warmings.

During the period from day 240 to day 270 the mean zonal wind shows stronger positive wind velocities in the composite of years with a major warming.

Apart of the stronger positive mean zonal wind in the beginning of the year in the composite of years with a major warming, the other differences between both composites cannot easily be explained by SSW effects. It is recommended to include stratospheric mean zonal wind data for further investigations.

Due to the stratospheric filtering described by e.g. *Lindzen* (1981), the gravity wave momentum flux in the mesosphere is expected to be negative in winter and

positive in summer. At heights above 85 km, this is confirmed for most at the time by the composite of the calculated momentum flux for years with a major warming (fig. 36). Apart from the occurrence of negative momentum flux in summer around day 210 and day 240 at heights of 85 km to 90 km, the composite of years without a major warming (fig. 35) shows also the annual variation.

Below 85 km the momentum flux is mainly positive over the entire year in the composite of years with a major warming. The untypical positive momentum flux in the first winter months up to 85 km is probably caused by negative zonal mean wind in the stratosphere due to the SSW. It was determined by MERRA data, that the period of negative stratospheric zonal mean wind lasts during the here considered SSW events at least 10 days. So it is a sufficient time period for the development of a strong positive momentum flux, which induces a positive wave drag. That wave drag accelerates the mean zonal wind, resulting in the observed enhancement of positive mean zonal wind from day 30 to day 60 (fig. 36). Due to the strong enhanced post SSW positive mean zonal wind, probably more gravity waves with positive velocities are filtered during the period from day 30 to day 60. Following the negative momentum flux above 88 km is stronger in the composite of years with a major warming than in the composite of years without a major warming. That would also explain the weaker positive mean zonal wind above 88 km in the composite of years with a major warming (fig. 36). The positive momentum flux in the last winter months up to 85 km in the composite of years with a major warming can hardly be explained by SSW processes.

The momentum flux in the composite of years without major warmings shows during the period from day 1 to day 60 and from day 330 to day 365 weak positive values ($u'w' < 3 \text{ m}^2/\text{s}^2$) as well as a weak negative momentum flux at heights from 78 km to 85 km. That momentum flux distribution meets more the expectations due to the filtering theory.

In both composites of the zonal mean wind the transition from negative to positive velocities in the upper summer mesosphere can be determined. That transition is probably caused by the strong positive momentum flux in summer which induces a positive wave drag. Note that the zero line of the zonal mean wind is located at larger heights of up to 100 km around day 120 and sinks with time.

The interaction between wave drag and mean flow is quite apparent in the upper summer mesosphere, since the appearance of positive momentum flux in summer coincides with the trend of the zero line of the mean zonal wind. Once the mean zonal wind in the upper mesosphere has turned to positive direction, a negative momentum flux dominates due to the changed filtering conditions. It is expected, that the positive zonal mean wind in the upper summer mesosphere weakens with height, because the negative momentum flux induces a negative wave drag, which decelerate the mean flow. That cannot be verified in the recent thesis, since it is not possible to determine reliable wind above 100 km by meteor radar for the data used in this study.

Further analyses should concern stratospheric mean zonal wind and gravity wave momentum flux, for the better identification of a vertical coupling. Note, that the windanalysis which is required for the momentum flux calculation, does not take into account shorter-period planetary waves as the 4-day and 5-day planetary wave. According to *Fedulina et al. (2004)* those waves are present in the stratosphere during most of the year. They have increased amplitudes during the spring time transition, in August-September and October-November. Especially during that periods daily changes due to the 4-day and 5-day planetary wave are probably not neglectable small, as it is assumed in the windanalysis (see chapter 3.4). This could be one explanation for the strong positive momentum flux up to 85 km in the latter winter months in both composites (fig. 35 and fig. 36).

6 Conclusion

In the present thesis the gravity wave activity in the mesosphere during major SSWs are investigated. The mesospheric gravity wave momentum flux and the mean zonal wind during major SSWs are analyzed. Furthermore, the annual variation of the gravity wave momentum flux and mean zonal wind in the mesosphere is compared for years with and without major warmings.

The variance of the fluctuations in the radial velocity is assumed to be a proxy for gravity wave activity. The discussion of the gravity wave activity in Andenes during the period ± 10 days around the SSW onset at heights from 78 km to 100 km showed an enhanced gravity wave activity before the SSW onset in 2004, 2006 and 2010. In those years the enhanced gravity wave activity weakens from the SSW onset on. That weakening of gravity wave activity during SSWs is also described in *Wang and Alexander (2009)*. The gravity wave activity distribution for the SSWs in 2009 and 2013 looked different. Therefore the activity distributions for the same height region and periods for Juliusruh were considered. A relation between the position of the radar related to the polar vortex and the strength of gravity wave activity is determined. When the polar vortex edge was located close to Andenes, strong gravity wave activity is observed. In turn, the gravity wave activity was particularly low, when Andenes was located close to the polar vortex center or outside of the polar vortex. These observations coincides with observations described by *Wang and Alexander (2009)* or *Whiteway et al. (1997)*. It can be summarized, that the gravity wave activity in the mesosphere in general is enhanced before the SSW onset and weakens during the SSW. But the position of the polar vortex has a strong impact on the gravity wave activity as well and is able to enhance the gravity wave activity significantly.

Contrary to expectations, no relation between gravity wave activity and strength or distribution of the gravity wave momentum flux could be established. That can be explained by the fact, that an increased gravity wave activity does not necessarily mean wave breaking and hence a momentum flux transfer. A possible relation between gravity wave activity and momentum flux could made out, if the gravity wave activity at stratospheric heights would be taken into account also.

Bear in mind that the variance of the fluctuations in the radial velocity contains the meridional wind component as well. Thus a large variance does not necessarily mean strong fluctuations in the mean zonal wind. However, the variance of the fluctuations in the radial velocity is still an established indicator for gravity wave activity.

The mesospheric wind and gravity wave momentum flux are calculated by data provided by the meteor radars at Andenes and Juliusruh. The gravity wave momentum flux was calculated by the established Hocking method (*Hocking (2005)*). For this a fit of the radial velocity is needed. That one is determined in the present thesis by a new approach, the adaptive spectral filtering. Here the several tidal components are subsequently fitted applying separate windows, which are adapted to the tidal period. After a tide component is fitted, it is removed from the wind. Then the next shorter period tide component is fitted from the residual wind. The entire procedure is repeated in one hour steps. That method ensures, that the fit of the several tides is not distorted by the other tidal components. However, that tide fit does not include the lunar tides and planetary waves (periods 2-5 days). As it found out by *Chau et al. (2015)* the semidiurnal lunar tide peaks during SSWs. For analysis during SSWs it is recommended to include at least the semidiurnal lunar tide in the tide fit. For this purpose it is necessary, that the lunar tide has an almost constant phase, so that the semidiurnal tide (period 12 h) and the semidiurnal lunar tide (period 12.42 h) can be distinguished from each other without any problems. However a constant phase of the semidiurnal lunar tide is not certain, since for the fit of amplitudes and phases a fitting window of at least 21 days is necessary (*Chau et al. (2015)*). That varying phase will probably create some difficulties by including the lunar tide in the windfit. Since the planetary waves (period 2-5 days) reach their maximum amplitudes mainly during seasonal transitions (*Fedulina et al. (2004)*), they should be included in the wind fit when annual variations are considered.

The momentum flux for the period ± 30 day centered around the SSW onset is averaged over 10 days and shifted by one day. Since the SSW is a short event, which lasts just a couple of days, small shifting steps as 1 day are recommended.

For the consideration of the momentum flux annual variation, it was averaged over 20 days and shifted by 10 days. In doing so an annual variation trend could be made out. For a better Nyquist ratio the averaging window should be expanded and the shifting steps should be shortened, e.g. an averaging window of 28 days and shifted by 7 days.

The onset of a SSW event was defined by the zonal wind reversal at the 10 hPa level as it is stated in *Labitzke and Naujokat (2000)*. In case of a major warming the wind reversal is still seen all over mesospheric heights. That could be confirmed by the mesospheric mean zonal wind in the present thesis, which shows mostly a clear wind reversal. For special cases as in 2010, mean zonal wind data for the 10 hPa level provided by MERRA were considered. For most of the considered years an enhancement of the positive post SSW mean zonal wind was observed. The strength of that enhancement correlates with the duration of the period of negative mean zonal wind at 10 hPa (MERRA data). That circumstance supports the theory, that the enhancement of positive post SSW wind is caused by a strong positive wave drag induced by positive gravity wave momentum flux. The positive momentum flux released by breaking gravity waves could develop well due to the long period of negative stratospheric wind. It is assumed, that the negative stratospheric wind filters gravity waves with negative phase velocities. The enhanced positive post SSW mean zonal wind in the mesosphere, in turn, filters vertical propagating waves with positive phase velocities. This results in the observed negative momentum flux some days after the SSW onset at heights above 85 km. The theory of gravity wave filtering by stratospheric winds is also supported by the momentum flux distribution before and after a SSW event in general. Furthermore it was observed, that the momentum flux varies strongly with height and to a smaller degree in time. So layers with small vertical dimensions and altering positive and negative momentum flux evolve. That could be explained by wave breaking and secondary wave generation (*Lindzen (1981)*).

At the end, the composites of the mesospheric annual mean zonal wind and gravity wave momentum flux in years with and without a major warming were compared. Both have in common, that the momentum flux distribution supports

in general the theory of gravity wave filtering by stratospheric winds, especially above 85 km. Moreover both composites show that the interaction between wave drag and mean flow is quite apparent in the upper summer mesosphere, since the appearance of positive momentum flux in summer coincides with the trend of the zero line of the mean zonal wind.

The most apparent difference between both composites is the strong enhanced positive mean zonal wind in years with a major warming during the period from day 30 to day 60 of the year. That circumstance is probably caused by the strong positive momentum flux during that period at heights up to 85 km, which is related with SSW processes. Under undisturbed conditions the momentum flux is expected to be negative during wintertime. In the composite of years with a major warming such a typical negative momentum flux in winter could not be observed at heights below 85 km.

Furthermore the composite of years with major warmings shows a stronger positive momentum flux in summer than the composite of years without major warmings. That could be an explanation for the stronger positive amplitudes of the mean zonal wind from day 240 to day 270.

Apart from the strong enhanced positive mean zonal wind and stronger positive momentum flux in the beginning of the year in the composite of years with a major warming, the other differences in the both composites cannot be explained by any relation to SSWs processes. For further analysis the stratospheric mean zonal wind and gravity wave momentum flux should be taken into account. In addition it is recommended to include the 4-day and 5-day planetary wave and the semidiurnal lunar tide in the windanalysis. Then fluctuations in the radial velocity can be assigned with greater certainty to gravity waves and the gravity wave momentum flux can be estimated more exactly.

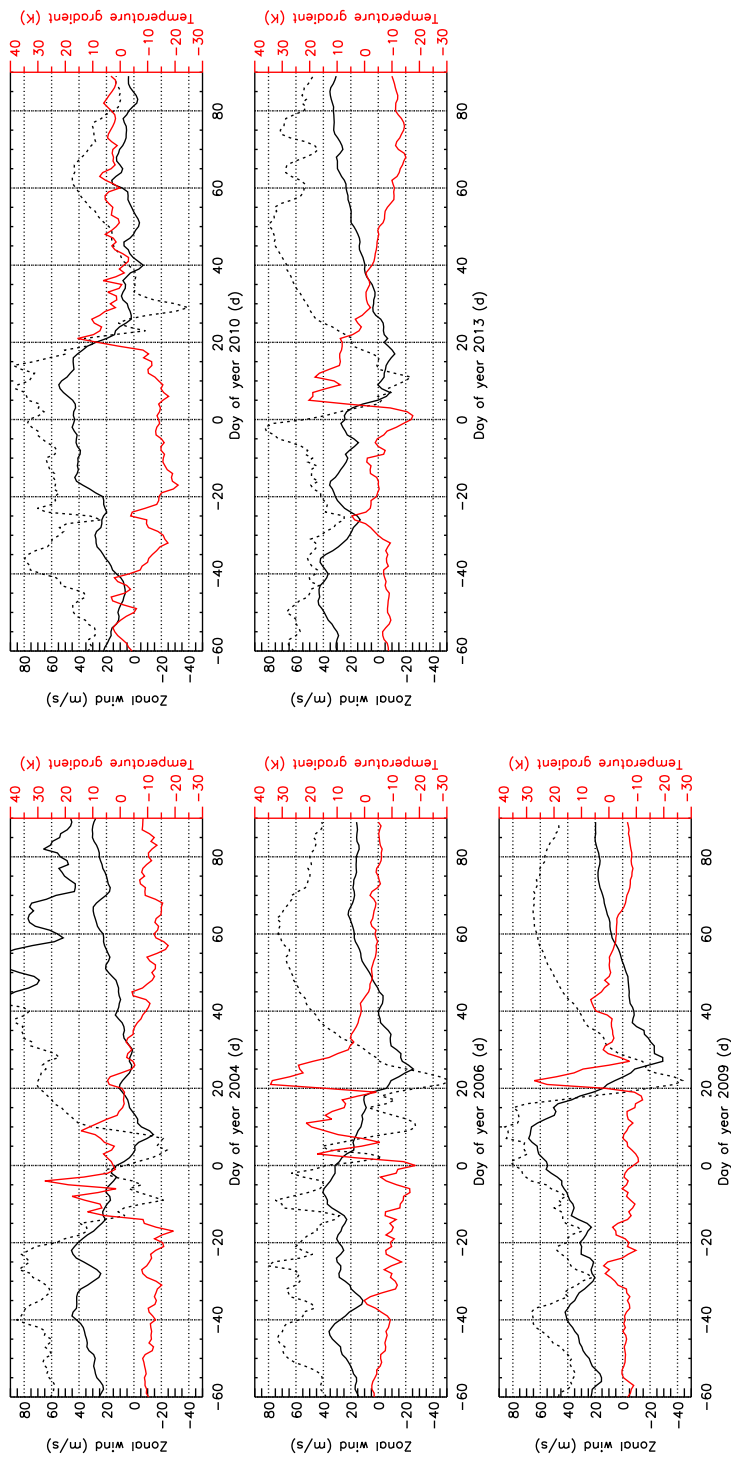


Figure 37: Mean zonal wind in 10 hPa (black solid line) and in 1 hPa (dashed line) and temperature in 10 hPa (red line) derived from MERRA data.

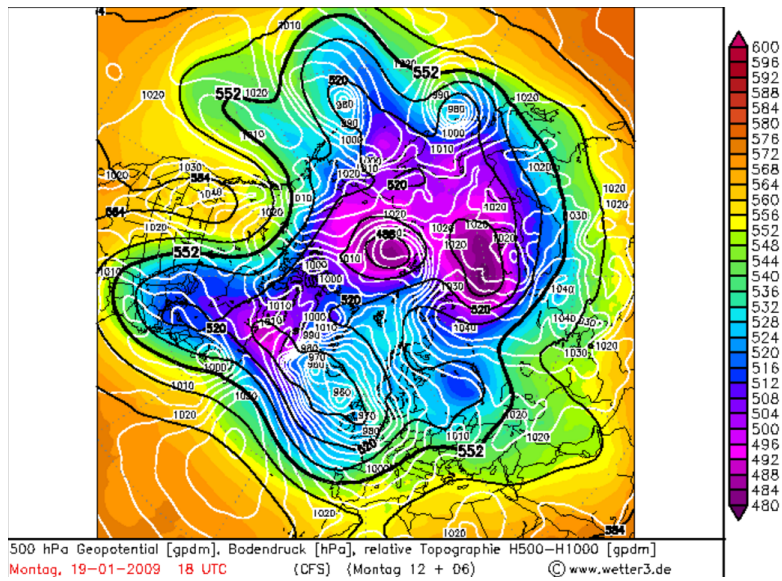


Figure 38: Position of polar vortex at the 19.01.2009
 taken from <http://ww1.wetter3.de/Archiv/>

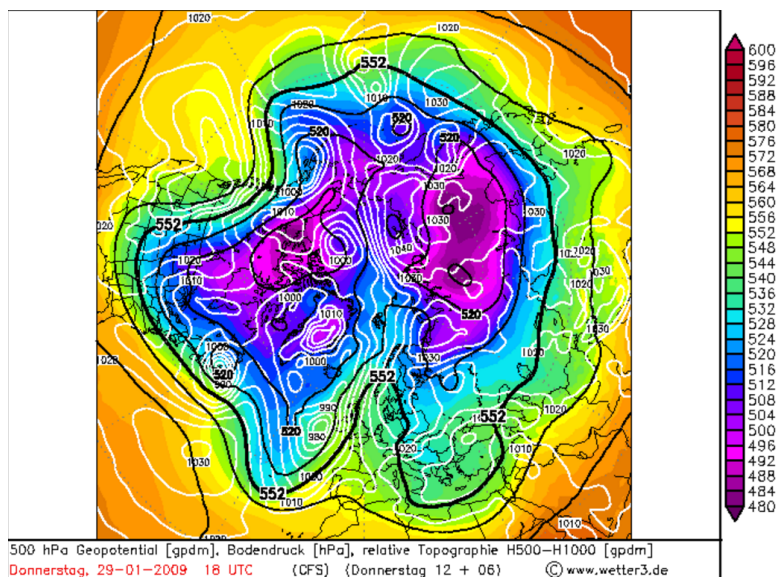


Figure 39: Position of the polar vortex at the 29.01.2009
 taken from <http://ww1.wetter3.de/Archiv/>

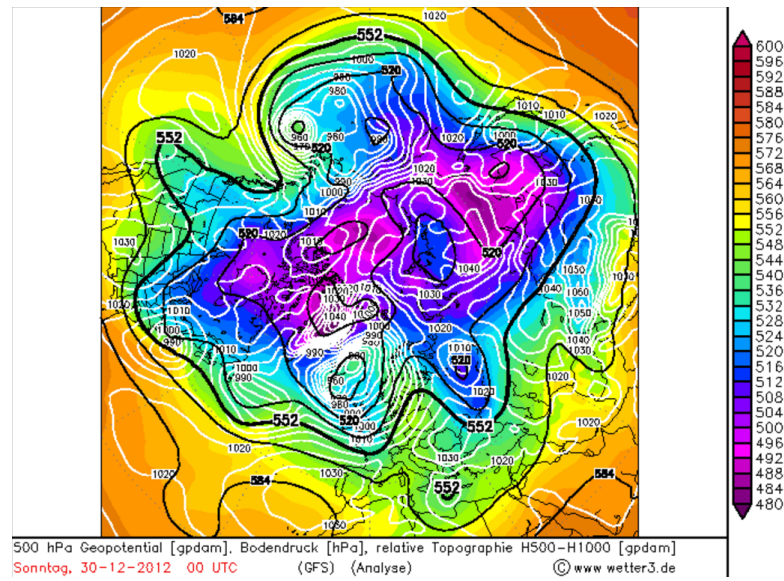


Figure 40: Position of the polar vortex at the 30.12.2012
 taken from <http://www1.wetter3.de/Archiv/>

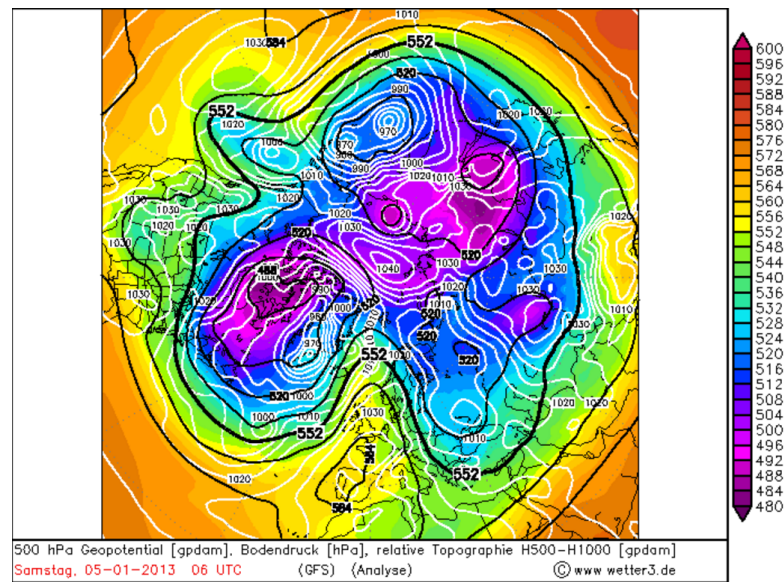


Figure 41: Position of the polar vortex at the 05.01.2013
 taken from <http://www1.wetter3.de/Archiv/>

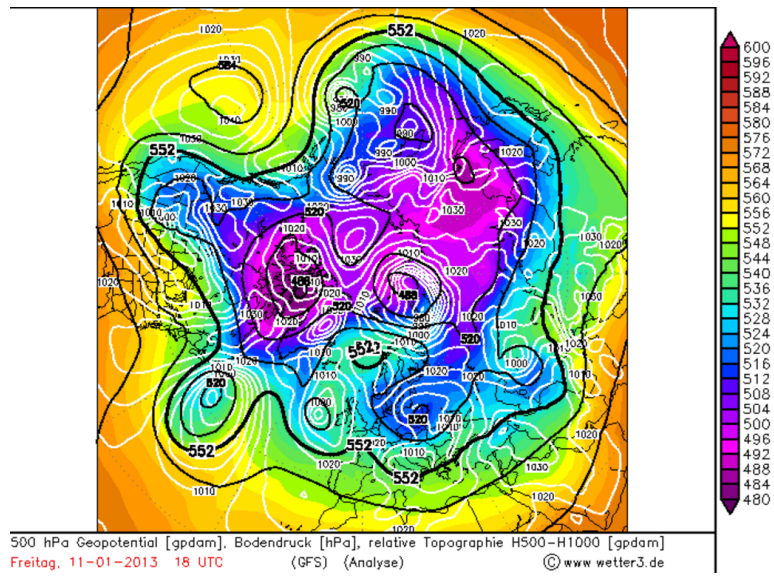


Figure 42: Position of the polar vortex at the 11.01.2013
 taken from <http://www1.wetter3.de/Archiv/>

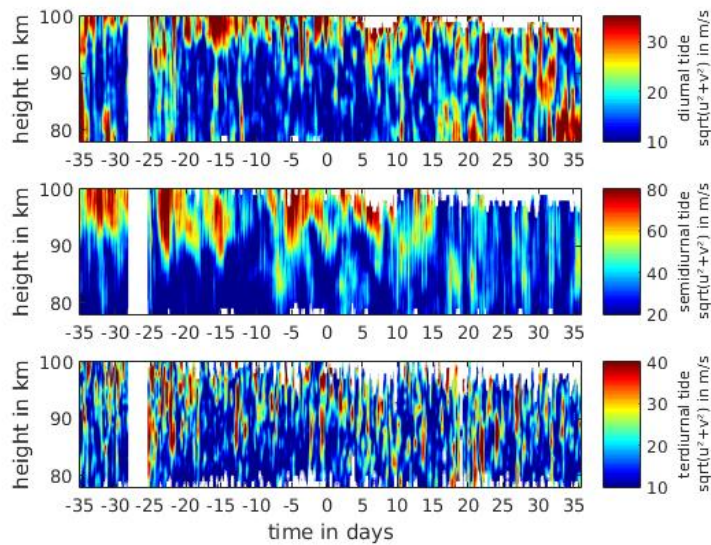


Figure 43: Terdiurnal tide (upper panel), semidiurnal tide (middle panel) and diurnal tide (lower panel) in the period from ± 30 days around the SSW 2004 onset (06.01.2004).

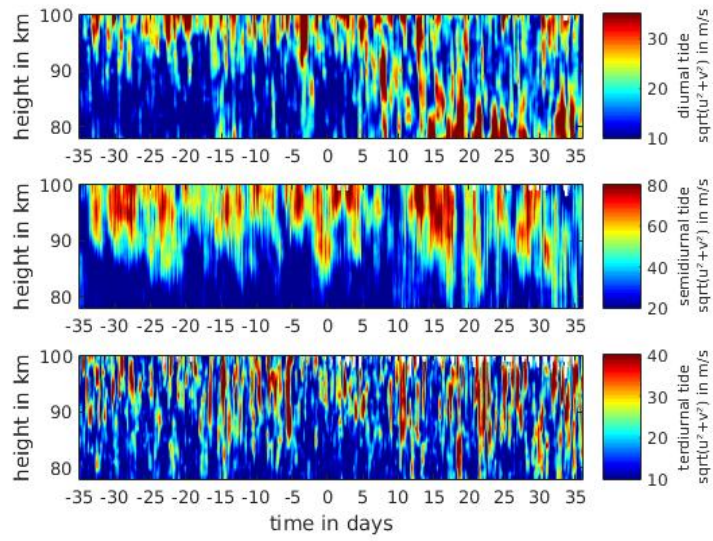


Figure 44: Terdiurnal tide (upper panel), semidiurnal tide (middle panel) and diurnal tide (lower panel) in the period from ± 30 days around the SSW 2006 onset (20.01.2006).

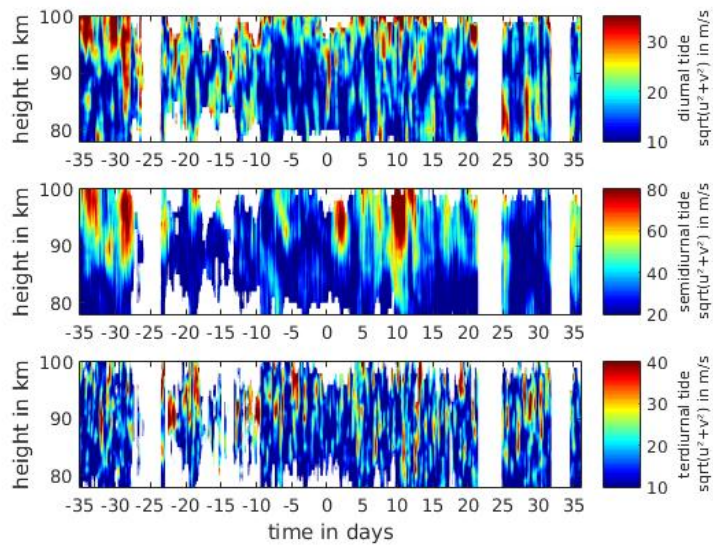


Figure 45: Terdiurnal tide (upper panel), semidiurnal tide (middle panel) and diurnal tide (lower panel) in the period from ± 30 days around the SSW 2009 onset (23.01.2009).

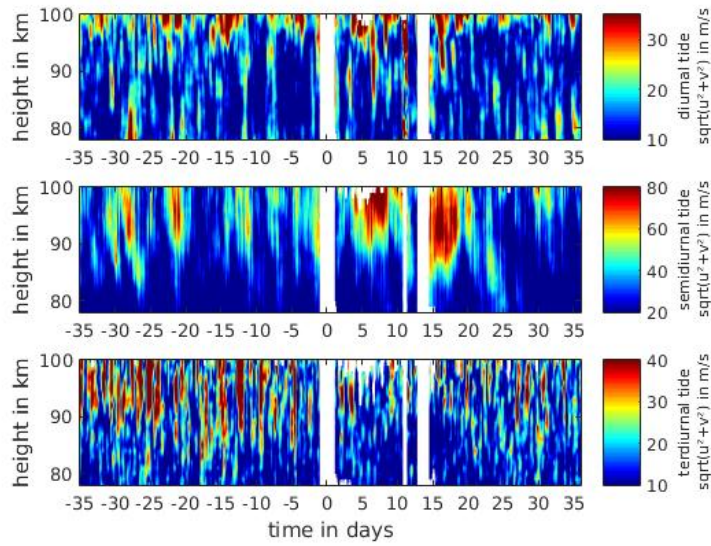


Figure 46: Terdiurnal tide (upper panel), semidiurnal tide (middle panel) and diurnal tide (lower panel) in the period from ± 30 days around the SSW 2010 onset (28.01.2010).

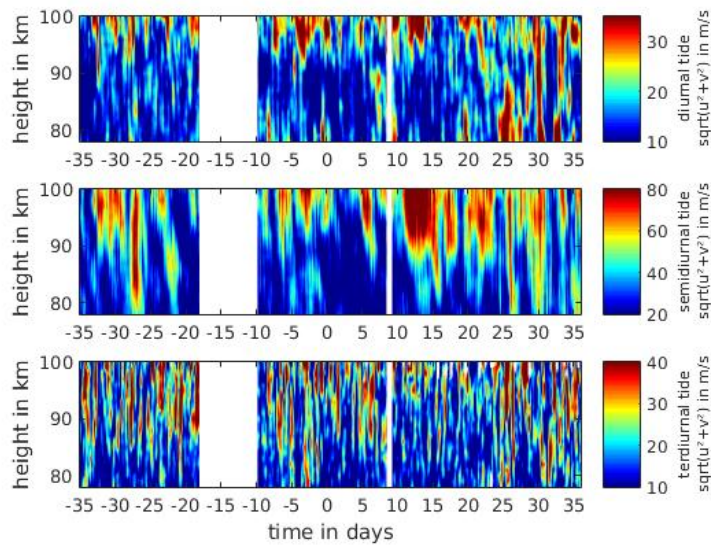


Figure 47: Terdiurnal tide (upper panel), semidiurnal tide (middle panel) and diurnal tide (lower panel) in the period from ± 30 days around the SSW 2013 onset (07.01.2013).

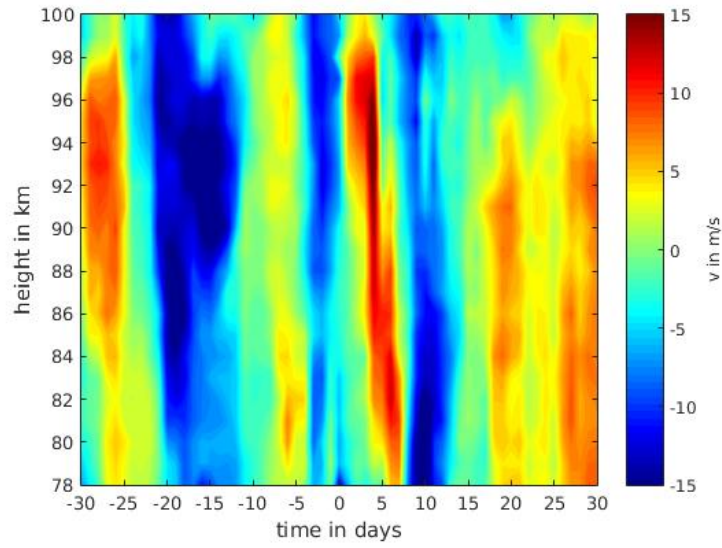


Figure 48: Composite of the mean meridional wind in the period from ± 30 days around the SSW onset of the years 2004, 2006, 2009, 2010 and 2013.

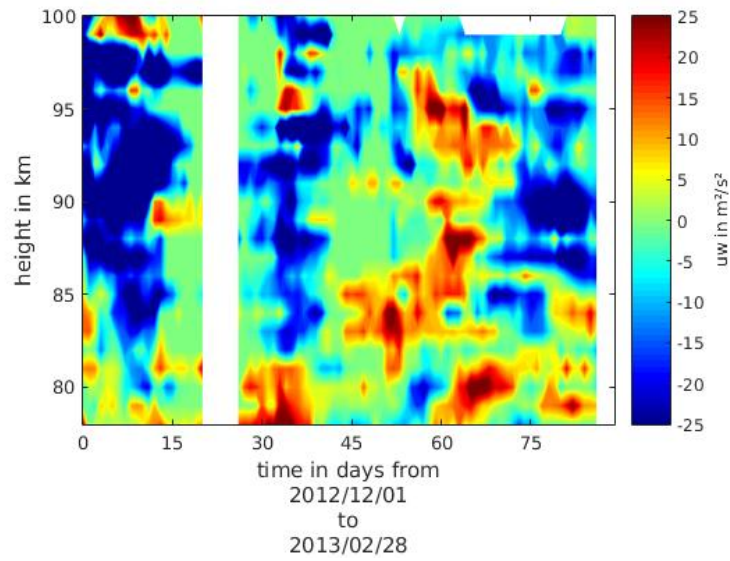


Figure 49: 10-day averaged 1-day shifted momentum flux, calculated with the same minimum amount of meteor events (30) and for the same period as in *de Wit et al.* (2014)

8 Bibliography

- Andrews, D. G., J. R. Holton, and C. B. Leovy, Middle atmosphere dynamics, *Quarterly Journal of the Royal Meteorological Society*, 115(486), 421–422, doi:10.1002/qj.49711548612, 1989.
- Andrioli, V. F., D. C. Fritts, P. P. Batista, and B. R. Clemesha, Improved analysis of all-sky meteor radar measurements of gravity wave variances and momentum fluxes, *Ann. Geophys*, 31, doi:10.5194/angeo-31-889-2013, 2013.
- Antonita, T. M., G. Ramkumar, K. K. Kumar, and V. Deepa, Meteor wind radar observations of gravity wave momentum fluxes and their forcing toward the Mesospheric Semiannual Oscillation, *Journal of Geophysical Research: Atmospheres*, 113(D10), n/a–n/a, doi:10.1029/2007JD009089, d10115, 2008.
- Brasseur, G. P., and S. Solomon, Aeronomy of the Middle Atmosphere, *Springer, Dordrecht, Netherlands, 3rd. ed*, 2005.
- Charney, J. G., and P. G. Drazin, Propagation of planetary-scale disturbances from the lower into the upper atmosphere, *Journal of Geophysical Research*, 66(1), 83–109, doi:10.1029/JZ066i001p00083, 1961.
- Chau, J. L., P. Hoffmann, N. M. Pedatella, V. Matthias, and G. Stober, Upper mesospheric lunar tides over middle and high latitudes during sudden stratospheric warming events, *Journal of Geophysical Research: Space Physics*, 120(4), 3084–3096, doi:10.1002/2015JA020998, 2015JA020998, 2015.
- de Wit, R. J., R. E. Hibbins, P. J. Espy, Y. J. Orsolini, V. Limpasuvan, and D. E. Kinnison, Observations of gravity wave forcing of the mesopause region during the January 2013 major Sudden Stratospheric Warming, *Geophysical Research Letters*, 41(13), 4745–4752, doi:10.1002/2014GL060501, 2014.
- Fedulina, I. N., A. I. Pogoreltsev, and G. Vaughan, Seasonal, interannual and short-term variability of planetary waves in Met Office stratospheric assimilated fields, *Q. J. R. Meteorol. Soc*, 130, 2445–2458, doi:256/qj.02.200, 2004.

- Forbes, J. M., Atmospheric tides: 1. Model description and results for the solar diurnal component, *Journal of Geophysical Research: Space Physics*, 87(A7), 5222–5240, doi:10.1029/JA087iA07p05222, 1982.
- Forbes, J. M., Tidal and Planetary Waves, *Journal of Geophysical Research: Space Physics*, 87, doi:10.1029/GM087p0067, 1995.
- Fritts, D. C., and M. J. Alexander, Gravity wave dynamics and effects in the middle atmosphere, *Reviews of Geophysics*, 41(1), n/a–n/a, doi:10.1029/2001RG000106, 1003, 2003.
- Hervig, M., R. E. Thompson, M. McHugh, L. L. Gordley, J. M. Russell, and M. E. Summers, First confirmation that water ice is the primary component of polar mesospheric clouds, *Geophysical Research Letters*, 28(6), 971–974, doi:10.1029/2000GL012104, 2001.
- Hocking, W. K., A new approach to momentum flux determinations using skyrimet meteor radars, *Annales Geophysicae*, 23(7), 2433–2439, doi:10.5194/angeo-23-2433-2005, 2005.
- Hocking, W. K., B. Fuller, and B. Vandeppeer, Real-time determination of meteor-related parameters utilizing modern digital technology, *Journal of Atmospheric and Solar-Terrestrial Physics*, 63(2-3), doi:http://dx.doi.org/10.1016/S1364-6826(00)00138-3, 2001.
- Hoffmann, P., W. Singer, D. Keuer, W. Hocking, M. Kunze, and Y. Murayama, Latitudinal and longitudinal variability of mesospheric winds and temperatures during stratospheric warming events, *Journal of Atmospheric and Solar-Terrestrial Physics*, 69(17–18), 2355 – 2366, doi:http://dx.doi.org/10.1016/j.jastp.2007.06.010, vertical Coupling in the Atmosphere/Ionosphere System3rd IAGA/ICMA Workshop, 2007.
- Holton, J. R., and M. J. Alexander, The Role of Waves in the Transport Circulation of the Middle Atmosphere, pp. 21–35, doi:10.1029/GM123p0021, 2000.

- Körnich, H., and E. Becker, A simple model for the interhemispheric coupling of the middle atmosphere circulation, *Advances in Space Research*, 45(5), 661 – 668, doi:http://dx.doi.org/10.1016/j.asr.2009.11.001, 2010.
- Labitzke, K., Temperature Changes in the Mesosphere and Stratosphere Connected with Circulation Changes in Winter, *Journal of the Atmospheric Sciences*, 29(4), 756–766, doi:10.1175/1520-0469(1972)029<0756:TCITMA>2.0.CO;2, 1972.
- Labitzke, K., and B. Naujokat, The lower arctic stratosphere in winter since 1952, *SPARC Newsletter*, 15:11–14,, 2000.
- Lindzen, R. S., Turbulence and stress owing to gravity wave and tidal breakdown, *Journal of Geophysical Research: Oceans*, 86(C10), 9707–9714, doi:10.1029/JC086iC10p09707, 1981.
- Longuet-Higgins, L., The Eigenfunctions of Laplace’s Tidal Equations over a Sphere, *Philosophical Transactions of the Royal Society of London. Series A, Mathematical and Physical Sciences*, 262(1132), 511–607, 1968.
- Lossow, S., Bestimmung von Schwerewellen-Parametern aus Temperaturprofilen gemessen mit einem Lidar in Nord-Norwegen im Sommer 2002, *University Berlin, Diplomarbeit*, 2003.
- Lübken, F.-J., and U. von Zahn, Thermal structure of the mesopause region at polar latitudes, *Journal of Geophysical Research: Atmospheres*, 96(D11), 20,841–20,857, doi:10.1029/91JD02018, 1991.
- Mager, F., Untersuchung der Anregung und Ausbreitung planetarer wellen in meteorologischen Analysen und einem Klima-Chemie-Modell, *University of Potsdam, Dissertation*, 2004.
- Matsuno, T., A Dynamical Model of the Stratospheric Sudden Warming, *Journal of the Atmospheric Sciences*, 28, 1971.
- Matthias, V., The role of planetary waves in coupling processes of the middle atmosphere, *University of Rostock, Dissertation*, 2014.

- McGraw, Concise Encyclopedia of Science and Technology, 1, 2009.
- Placke, M., Dissertation, Gravity waves and momentum fluxes in the mesosphere and lower thermosphere region, *University of Rostock, Dissertation*, 2014.
- Placke, M., P. Hoffmann, E. Becker, C. Jacobi, W. Singer, and M. Rapp, Gravity wave momentum fluxes in the MLT—Part ii: Meteor radar investigations at high and midlatitudes in comparison with modeling studies, *Journal of Atmospheric and Solar-Terrestrial Physics*, 73(9), 911 – 920, doi:<http://dx.doi.org/10.1016/j.jastp.2010.05.007>, scientific Results from Networked and Multi-instrument studies based on {MST} Radar, 2011.
- Rapp, M., and F.-J. Lübken, On the nature of PMSE: Electron diffusion in the vicinity of charged particles revisited, *Journal of Geophysical Research: Atmospheres*, 108(D8), n/a–n/a, doi:10.1029/2002JD002857, 8437, 2003.
- Richards, M., Fundamentals of Radar Signal Processing, *McGraw-Hill Electronic Engineering Series*.
- Rosby, c.-G., Relation between variations in the intensity of the zonal circulation of the atmosphere and the displacements of the semipermanent centers of action, *J.Mar. Res*, 2(38), 1939.
- Sato, T., Radar principles, *Handbook for MAP*, 30.
- Scherhag, R., Die explosionsartige stratosphärenenerwärmung des spätwinters 1951/52, *Ber. Deut. Wetterdienst*, 38, 1952.
- Skolnik, M., Radar Handbook, *McGraw-Hill Professional*, 2.
- Stober, G., Astrophysical Studies on Meteors using a SKiYMET All-Sky meteor radar, *University Leipzig, Dissertation*, 2009.
- Venkat Ratnam, M., T. Tsuda, C. Jacobi, and Y. Aoyama, Enhancement of gravity wave activity observed during a major southern hemisphere stratospheric warming by champ/gps measurements, *Geophysical Research Letters*, 31(16), n/a–n/a, doi:10.1029/2004GL019789, 116101, 2004.

- Vincent, R. A., and I. M. Reid, HF Doppler Measurements of Mesospheric Gravity Wave Momentum Fluxes, *J. Atmos. Sci.*, 40(5), doi:1321-1333, 1983.
- Wang, L., and M. J. Alexander, Gravity wave activity during stratospheric sudden warmings in the 2007–2008 northern hemisphere winter, *Journal of Geophysical Research: Atmospheres*, 114(D18), n/a–n/a, doi:10.1029/2009JD011867, d18108, 2009.
- Whiteway, J. A., T. J. Duck, D. P. Donovan, J. C. Bird, S. R. Pal, and A. I. Carswell, Measurements of gravity wave activity within and around the Arctic stratospheric vortex, *Geophysical Research Letters*, 24(11), 1387–1390, doi:10.1029/97GL01322, 1997.
- Yamashita, C., H.-L. Liu, and X. Chu, Gravity wave variations during the 2009 stratospheric sudden warming as revealed by ECMWF-T799 and observations, *Geophysical Research Letters*, 37(22), n/a–n/a, doi:10.1029/2010GL045437, l22806, 2010.

Danksagung

An dieser Stelle möchte ich Herrn Prof. Chau danken, dass er mir ermöglicht hat die Arbeit in der Radarabteilung am IAP anzufertigen.

Mein besonderer Dank geht an meinen Betreuer Dr. Gunter Stober und an Dr. Vivien Matthias die mir stets mit Rat und Tat bis zur letzten Sekunde zur Seite standen und auch in schwierigen Zeiten immer aufmunternde Worte für mich parat hatten.

Ein weiterer Dank geht an meine Kollegen in der Radarabteilung, die für eine sehr schöne Arbeitsatmosphäre gesorgt haben. Hervorheben möchte ich hier auch noch meinen Dank an Svenja Sommer und Rosemarie von Rein, die immer ein offenes Ohr für mich hatten.

Doch selbst mit der großartigen Betreuung und Unterstützung seitens des IAPs hätte ich die Arbeit nicht ohne meinen Clemens schreiben können, der immer an mich geglaubt hat. Ich kann gar nicht schätzen wie viele Kilometer er mit dem Kinderwagen gemacht hat, damit ich in Ruhe meine Arbeit schreiben konnte. Meinen Dank kann ich kaum in Worte fassen.

Zuletzt aber dafür umso herzlicher danke ich Maren für ihre (Mitt)wöchentlichen Einsätze und meiner Familie, die mich immer unterstützt und motiviert haben.

Selbständigkeitserklärung

Ich versichere hiermit an Eides statt, dass ich die vorliegende Arbeit selbstständig angefertigt und ohne fremde Hilfe verfasst habe, keine außer den von mir angegebenen Hilfsmitteln und Quellen dazu verwendet habe und die den benutzten Werken inhaltlich und wörtlich entnommenen Stellen als solche kenntlich gemacht habe.

Rostock, den 26. August 2016

